*GEOLOGICA CARPATHICA*, FEBRUARY 2022, 73, 1, 63–79 https://doi.org/10.31577/GeolCarp.73.1.4

# The petrography and geochemistry of clastic rocks from the Upper Cretaceous Terani Formation of the Cauvery Basin, Southern India

SUBIN PRAKASH R.[1,2,✉], SOORIYAMUTHU RAMASAMY[1], JOHN S. ARMSTRONG-ALTRIN[3] and THIVYA CHANDRASEKAR[1]

[1]School of Earth Sciences, Department of Geology, University of Madras, Guindy campus, Chennai-600025, India; ✉suban5geo@gmail.com
[2] Department of Geology, Maharaja's College, Mahatma Gandhi University, Ernakulam, Kerala-682011, India
[3]Universidad Nacional Autónoma de México, Instituto de Ciencias del Mar y Limnología, Unidad de Procesos Oceánicos y Costeros, Ciudad Universitaria, Ciudad de México 04510 CDMX, México

*(Manuscript received April 21, 2020; accepted in revised form August 18, 2021; Associate Editor: Jozef Michalík)*

**Abstract:** The petrography and geochemistry of clastic rocks from the Upper Cretaceous Terani Formation of the Cauvery Basin were studied to decipher their intensity of weathering, provenance, and tectonic history. Texturally, the Terani sandstones are moderately sorted with sub-angular and sub-rounded grains, indicating short transport and low maturity. The average Quartz–Feldspar–Rock fragment (Q–F–R) ratio of the Terani sandstone is $Q_{89}$–$F_3$–$R_8$. Geochemically, the Terani clastic rocks are classified as sublitharenites, Fe-sand, shale, and Fe-shale types. The chemical index of alteration (CIA), plagioclase index of alteration (PIA), and chemical index of weathering (CIW) suggested moderate to high intensity of weathering in the source area. The enrichment of rare earth element (REE) contents in the Terani clastic rocks relative to UCC (Upper Continental Crust) indicates a higher concentration of heavy minerals. Likewise, the average values of $Eu/Eu^*$ (0.16), La/Sc (2.94), La/Co (2.15), Th/Sc (1.08), Th/Co (0.79), Th/Cr (0.12), and Cr/Th (8.39) revealed that the Terani clastic rocks were derived from a combination of felsic and intermediate source rocks. The chondrite normalized REE patterns of clastic rocks are characterized by a relatively flat HREE ($Gd_{cn}/Yb_{cn}$=1.71), enriched LREE ($La_{cn}/Sm_{cn}$=4.15), and negative Eu anomaly ($Eu/Eu^*$=0.16), which suggest the contribution of sediments with less HREE depleted source rocks from the Archaean group. A comparison of the REE pattern and Eu anomalies from this study with potential source rocks infers that the Terani Formation received a major contribution of sediments from the Dharwar Craton.

**Keywords:** Dharwar Craton, petrography, geochemistry, weathering, provenance.

## Introduction

The composition of clastic rocks is influenced by the nature of the source rock, intensity of weathering, distance of transport, grains size, diagenesis, and sorting (McLennan et al. 1993; Ramos-Vázquez et al. 2017, 2018; Madhavaraju et al. 2020). However, the geochemical composition of clastic rocks has been widely used to infer the provenance (Rahman et al. 2014; Etemad-Saeed et al. 2015; Zeng et al 2020), weathering (Cullers 1994; Mustafa & Tobia 2020; Verlekar & Kotha 2020), and the tectonic history of the source area (Armstrong-Altrin 2015, 2020; Rivera-Gómez et al. 2020; Znad et al. 2020). Numerous studies have utilised the immobile trace (Y, Th, Zr, Nb, Sc, Co, Cr) and REE concentrations of clastic rocks as a tool for suggesting provenance due to their short residence time in seawater and stability during secondary processes, such as diagenesis and metamorphism (Cox et al. 1995; Dey et al. 2009; Armstrong-Altrin & Machain-Castillo 2016).

In the Cauvery Basin, the Upper Cretaceous Terani sedimentary succession (60 m thick) unconformably overlies the Archaean crystalline basement. The dispersal of sediments from this formation indicates that they were mostly derived from the Archaean basement rocks lying on the southern part of the Basin (Sundaram et al. 2001). Although some studies have been focused on the textural characteristics of the Upper Cretaceous clastic rocks (Madhavaraju & Lee 2010; Nagendra et al. 2011; Madhavaraju 2015; Krishnan et al. 2020), the petrography and geochemistry of the Terani Formation clastic rocks have not been studied sufficiently by other researchers. In order to fill in this knowledge gap, the provenance, weathering, and tectonic setting of the Terani clastic rocks, which are based on the petrography, major, trace, and REE geochemistry data, are discussed in this study. In addition, the REE patterns of granites and gneisses that are located relatively close to the study area (Dharwar Craton and Kerala Khondalite Belt) are compared with the clastic rocks of this study to infer the source rocks.

## Regional geological framework

The Cauvery Basin is considered to be a rift basin located along the eastern continental margin of the Peninsular India, which covers 25,000 km$^2$ of the Tamil Nadu State and extends

into the Bay of Bengal and the Gulf of Mannar (Biswas 1993; Prabhakar & Zutshi 1993). The Cauvery basin represents a passive margin near the southern part of India, which is formed as a result of the fragmentation of Gondwanaland during the Early Cretaceous and continued to evolve until the Tertiary through rift, pull–apart, shelf sag, and tilt phases (Prabhakar & Zutshi 1993). The sedimentary rocks of the Cauvery Basin were deposited in an elongate, narrow passage extending in an NNE–SSW direction, and its margins are demarcated by faults (except in the north), where the basin was connected to the open ocean (Sundaram & Rao 1986). They are well exposed in five areas, such as Pondicherry, Virudhachalam, Ariyalur, Tanjore, and Sivaganga (Fig. 1). Previous studies in the Cauvery Basin sediments were focused on sequence stratigraphy, paleontology, clay mineralogy, geochemistry, depositional environments, and tectonic evolution (Srivastava & Tewari 1967; Banerji 1972; Sastry et al. 1972; Sundaram & Rao 1986; Ramasamy & Banerji 1991; Govindan et al. 1996; Sundaram et al. 2001; Madhavaraju & Lee 2010). On the basis of lithology, a detailed stratigraphic study was carried out by Blanford (1862), and he divided the sedimentary formation into three groups: Uttatur, Trichinopoly, and Ariyalur in ascending order (Table 1). In some places, these three groups are unconformable, and this unconformable relationship represents the successive stages of marine transgression. Later, extensive studies were undertaken by Sundaram & Rao (1986) and Sundaram et al. (2001) on the Cretaceous–Paleocene rocks. Sundaram et al. (2001) divided the Uttatur Group into four formations: Terani, Arogyapuram, Dalmiapuram, and Karai Formations. The first three formations are considered Early Cretaceous, whereas the last formation is of Late Cretaceous age.

The Terani Formation is exposed in the Dalmia Ceramic (Bharath) Ltd. Kaolinite Quarry, 2 km NE of the village of Terani, and denoted here as the type sequence. The approximate thickness of this formation extends up to 60 m along the Archaean crystalline rocks. The Terani Formation has been extensively referred to in literature as the "Uttatur plant bed" or the "Upper Gondwana" (Tewari et al. 1996). Based on the Ptylophyllum plant fossil of the Early Cretaceous–Aptian age, it has been compared with the Terani Formation. The depositional environment reveals that it is fluviatile to paralic, which is characterized by bedded, fine-grained siliciclastic deposits in some exposures. These represent overbank fluvial and lacustrine deposits; however, they are not diagnostic of deltaic facies and are also likely to be represented in the assemblage. The Terani Formation is divided into two members: a lower sandstone member and an upper shale member (Ramasamy & Banerji 1991). The sandstone member consists of coarse-grained to very coarse-grained sandstone and boulder conglomerate. The sandstone member starts with a boulder bed overlying the Archaean basement rocks. The upper shale member includes kaolinitic claystone and micaceous shale (Ramasamy & Banerji 1991). The upper shale member is well-exposed in both the Terani and Teranipalayam clay mines (Ramasamy & Banerji 1991). Lithologically, the studied section consists of a thick sequence of clay, ferruginous sandstone, and calcrete beds with different colours (whitish clay, whitish red clay, whitish yellow clay and whitish brown clay) (Fig. 2).

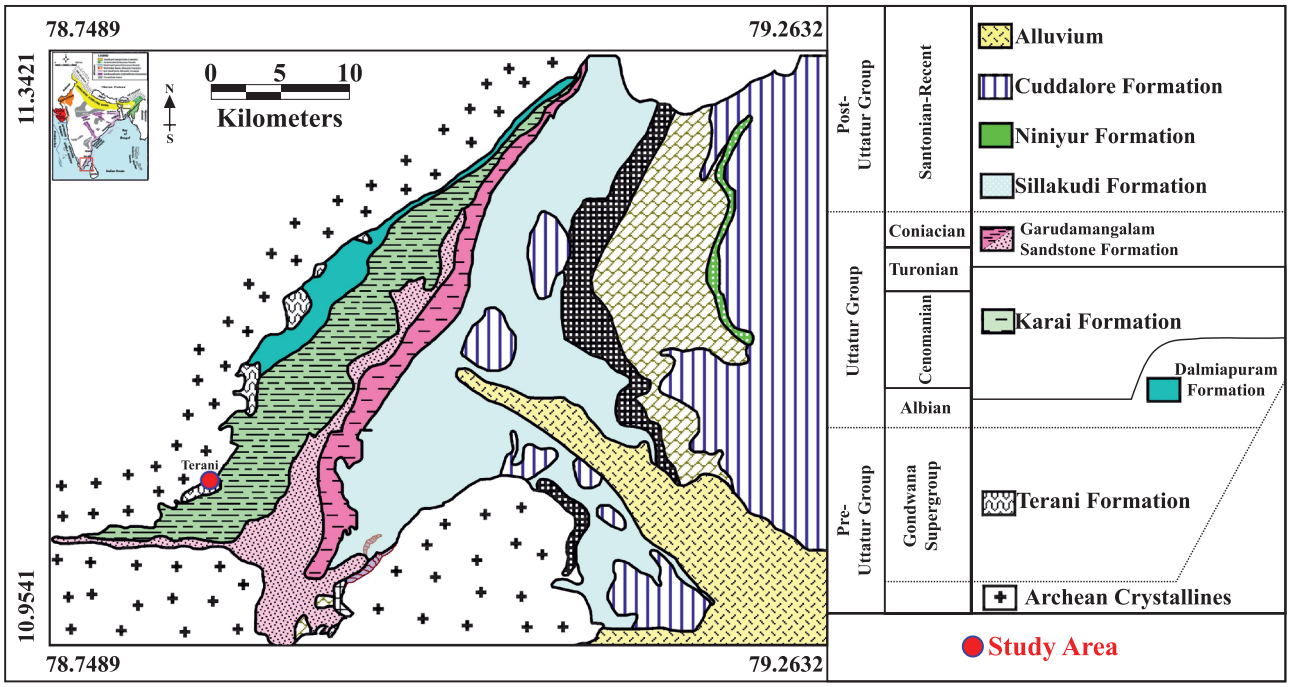


**Fig. 1.** Geological map showing the sample location of the Cretaceous outcrops of the onshore Cauvery Basin with stratigraphic elaborations to the right (modified after Sundaram et al. 2001).

## Analytical techniques

### *Petrography*

Well-sorted and less-weathered, fine to coarse-grained sandstone samples (number of samples n=10) were selected for modal analysis to minimize the grain size effect (Ingersoll et al. 1984). For k-feldspar identification, thin sections were stained with sodium cobalt nitrate (Carver 1971). For modal analysis, a minimum of 300 framework grains were counted from each thin section, except for the matrix and cement, by following the Gazzi–Dickinson (Ingersoll et al. 1984) and Indiana group methods (Suttner 1974; Basu 1976; Mack & Suttner 1977; Suttner et al. 1981).

### *Geochemistry*

A total of eighteen samples were selected from the Terani Formation for the determination of major, trace, and REE geochemistry. Approximately 10 g of the powdered sample was weighed on a microbalance (Sartorius; Model CP225D; weighing errors are of the order of ±0.05 mg) to determine Loss on Ignition (LOI). The powdered samples were heated in a muffle furnace for ignition at 900 °C for 4 hours, and the difference in weight was calculated to obtain the LOI. For XRF analysis, these ignited sample powders were analysed at the National Centre for Earth Science Studies (NCESS), Thiruvananthapuram. The average LOI values of the analysed Terani clastic rocks are ~6.67 %.

**Table 1:** Generalized lithostratigraphy of Cauvery Basin (Sundaram et al. 2001).

| Age | | Formation | Member | Thickness (m) |
|---|---|---|---|---|
| Mio-Pliocene | | Cuddalore Sandstone | | >150 |
| | | ..... Unconformity ..... | | |
| Danian | | Niniyur | Periyakurichchi Biostromal | 26 |
| | | | Anandavadi Arenaceous | 30 |
| | | ..... Unconformity ..... | | |
| | ARIYALUR GROUP | Kallamedu | | 100 |
| | | ..... Unconformity ..... | | |
| | | Ottakoil | | 40 |
| Maastrichtian | | ..... Unconformity ..... | | |
| | | Kallankurichchi | Srinivasapuram Gryphean Limestone | 18 |
| | | | Tancem Biostromal | 8 |
| | | | Kattupiringiyam Inoceramus Limestone | 8 |
| | | | Kallar Arenaceous | 6 |
| | | ..... Unconformity ..... | | |
| Campanian | | Sillakkudi | Varanavasi Sandstone | 270 |
| | | | Sadurbagam Pebbly Sandstone | 80 |
| Santonian | | | Varakuppai Lithoclastic Conglomerate | 45 |
| | | ..... Unconformity ..... | | |
| Coniacian | | Garudamangalam | Anaipadi Sandstone | 215 |
| | | | Grey Sandstone | 80 |
| | | | Kulakkanattam Sandstone | 45 |
| | | ..... Unconformity ..... | | |
| Turonian | | Karai | Odiyam Sandy Clay | 175 |
| | | | Gypsiferous Clay | 275 |
| | | ..... Unconformity ..... | | |
| Cenomanian | | Dalmiapuram | Kallakkudi Calcareous Sandstone | 60 |
| | | | Olaipadi Conglomerate | 65 |
| | | | Dalmia Bihermal Limestone | 15 |
| Albian | | | Varagupadi Biostromal Limestone | 23 |
| | | | Grey Shale | 7 |
| | | ..... Unconformity ..... | | |
| Aptian | | Terani | | 30 |
| | | Sivaganga | Kovandankurichchi Sandstone | 24 |
| Baremian | | | Basal Conglomerate | 18 |
| | | ..... Unconformity ..... | | |
| | | Archaean Granitic Gneiss | | |

To determine the trace and REE concentrations, the sample solutions were analysed using single collector High Resolution–Inductively Coupled Plasma Mass Spectrometry (HR–ICPMS; Nu Attom, UK) at the National Geophysical Research Institute (NGRI), Hyderabad. The acid digestion of powder samples was carried out following the method as described by Satyanarayanan et al. (2014) and Balaram (2020). The procedure for solution preparation for analysis is summarised below:

0.05 g of powdered rock sample was taken into a clean and dry Savillex Teflon pressure decomposition vessel. Afterwards, 10 ml of acid mixture of 7 parts of HF and 3 parts of $HNO_3$ were added to each sample and swirled thoroughly for complete moistening of the sample. The vessels were closed tightly and placed on a hot plate at 150 °C for 48 hours. Subsequently, the vessels were opened in a fume hood chamber and evaporated to near dryness. 1 ml of $HClO_4$ was added to the dried samples for the complete removal of HF by evaporation. The residue was dissolved with 10 ml of 1:1 $HNO_3$ and kept on the hot plate for 40 minutes for the complete dissolution of suspended particles. The solution was transferred to a 250 ml volumetric flask after cooling to room temperature. The volume consisted of 250 ml of purified water (18 MΩ) with the addition of 10 ml 1:1 $HNO_3$ and 5 ml of 1 ppm $^{103}Rh$ (acting as an internal standard). 10 ml of the solution was diluted to 50 ml in a volumetric flask with purified water (18 MΩ). The solution was stored in 60 ml HDPE sample bottle for analysis. These solutions were analysed using a single collector HR–ICPMS. The international standards (SRMs) GSR-5, GSR-4, JDO1, JG-2 and SCO-1 were used for reference. The replicate samples were measured during the analysis to determine the precision. Accuracy and precision of the determinations were better than 4–8 %. In this study, calcrete concentration was not used for geochemical

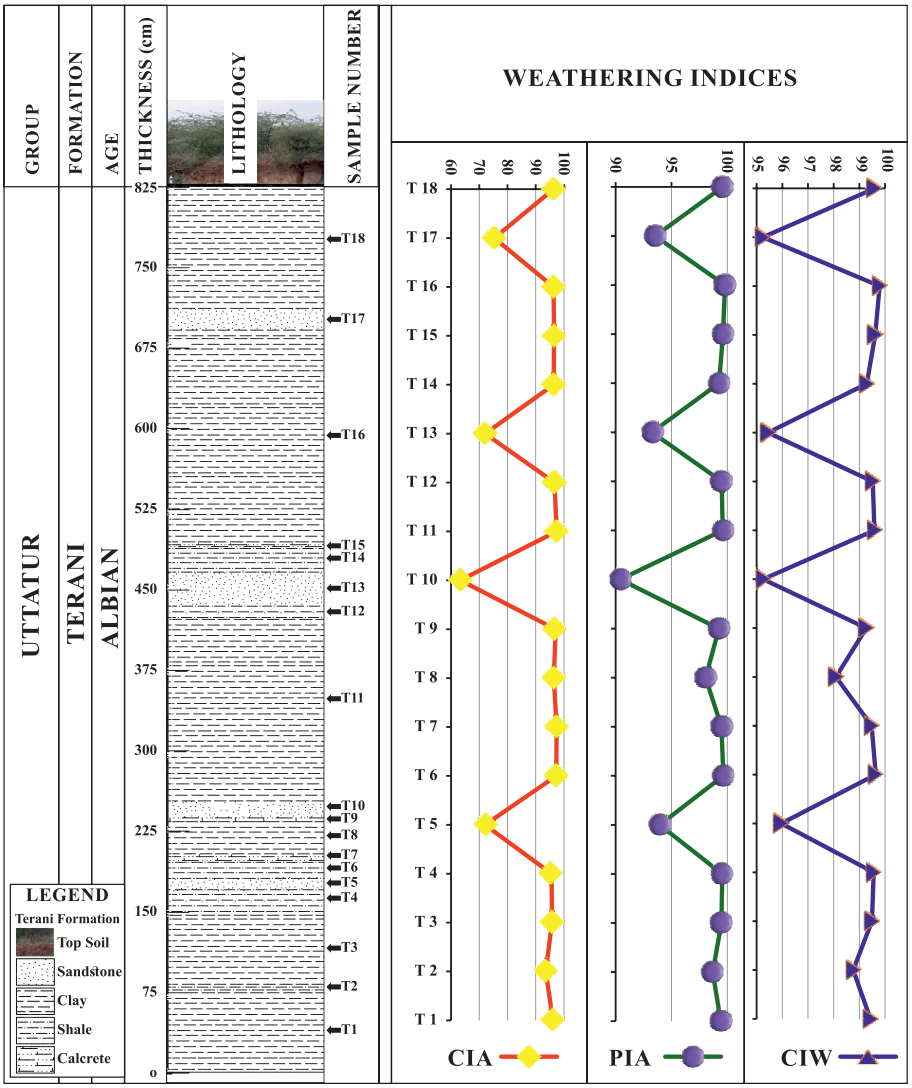


**Fig. 2.** Lithostratigraphic section of the Gondwana succession of the Terani Formation located near to Karai Clay Quarry.

interpretations. The geochemistry data were compared with the UCC (Upper Continental Crust) and PAAS (Post Archaean Australian Shale) values.

## Results

### *Petrography*

The detrital grains of the Terani sandstones are fine to coarse-grained, sub-angular to sub-rounded, and moderately-sorted to well-sorted (Fig. 3a–f). The sandstones are composed of quartz, feldspars, rock fragments, glauconite, opaque, and heavy minerals with ferruginous cement. The thin sections consist of mica, particularly biotite, which is more abundant than white mica in some samples. The main framework mineral, coarse-grained monocrystalline quartz exhibits undulatory and non-undulatory types (Fig. 3a). The polycrystalline quartz exhibits >5 crystal unit per grain, and some of the grains rarely show up to 3 crystal unit per grain with crenulated fabrics of low abundance (Fig. 3b; 3–16 %, Avg. 8). The microcline feldspar shows distinct cross-hatched twinning with alteration (Fig. 3c). Quartz grains with inclusions of heavy minerals, opaques, and vacuoles are abundant in many thin sections (Fig. 3d). Most of the quartz and feldspar grains are relatively fresh and unaltered. Rock fragments are relatively high in abundance as compared to plagioclase and K–feldspars. The sandstone is well-cemented by secondary authigenic quartz in the form of overgrowth, and the detrital grains are coated with a thin, red-brown rim of iron oxides (Fig. 3e). In a few of the thin sections, the outlines of the framework grains are irregular and wavy because of the pressure solution effect (Fig. 3f). Sandstones are generally moderately immature, lithic-dominated arenites with textures deciphering relatively few cycles of reworking.

The point-count data of sandstone shows enrichment of subangular–sub-rounded quartz grains (85–91 %, Table 2). Petrography analysis depicts monocrystalline quartz as the

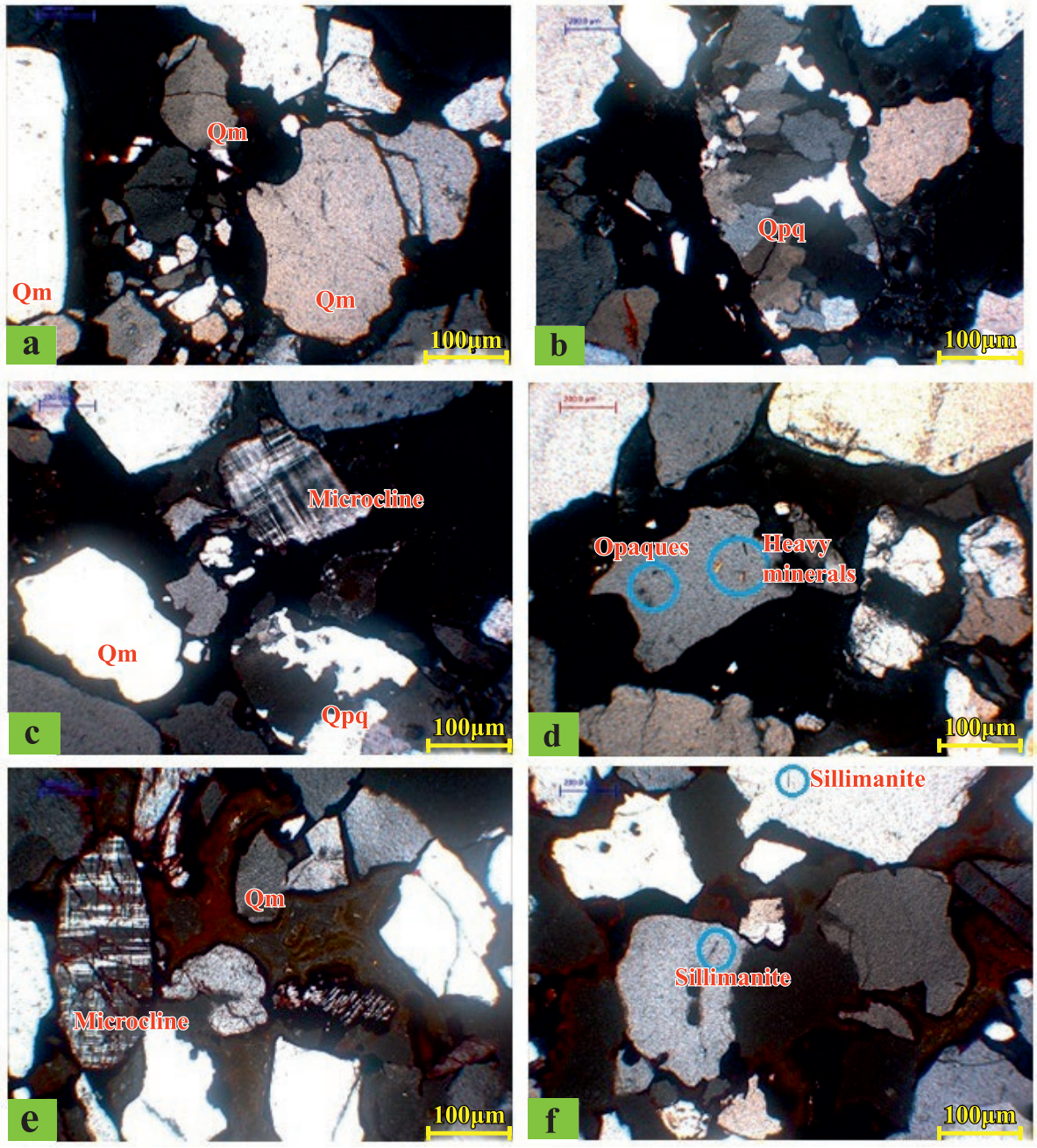


**Fig. 3.** Microphotographs of Terani sandstones: **a** — Monocrystalline quartz (Qm) with undulatory extinction; **b** — Polycrystalline quartz grains (Qpq) showing >5 crystal per grain with crenulated fabrics; **c** — Cross-hatched microcline feldspar with monocrystalline and polycrystalline quartz grains; **d** — Inclusions of heavy and opaque minerals in quartz grains; **e** — Quartz grains are coated with iron oxide cement; **f** — Pressure–solution effects on the outline of framework grains.

most dominant clasts (84–90 %) followed by rock fragments (6–11 %). Lithic fragments include igneous (e.g., granite) and metamorphic (e.g., schist and phyllite), which are relatively abundant to sedimentary rocks (e.g., chert). Sandstones contain a minor amount of feldspar (plagioclase and k-feldspar) (2–5, Avg. 3 %). Most of the thin sections contain a small amount of K-feldspars, including microcline (twinned). The average Q–F–R ratios of Terani sandstones are $Q_{89}$–$F_3$–$R_8$ respectively. In the ternary diagram by Dickinson (1985), sandstones were plotted in the recycled orogeny and craton interior fields (Fig. 4). The heavy mineral spectra of the analysed sandstone (n=4) are primarily dominated by ilmenite, zircon, magnetite, garnet, tourmaline, rutile, sillimanite, and kyanite of increasing order. The ultra-stable minerals (zircon, tourmaline, rutile) exhibit euhedral, pyramidal, and sub-rounded shapes.

Petrographically, Terani shales are fine-grained and contain a grey to greenish-grey, argillaceous matrix. Form the vestiges

**Table 2:** Recalculated modal point counts of the Terani Formation – Cauvery Basin sandstone samples based on Dickinson (1985).

| TERANI FORMATION | | | | | | | | | | | | | | | | | |
|---|---|---|---|---|---|---|---|---|---|---|---|---|---|---|---|---|---|
| Sl. No. | Samples | Sample Type | Q (%) | F (%) | R (%) | Qm (%) | F (%) | Rt (%) | Qt (%) | F (%) | Rt (%) | Qpq (%) | F (%) | R (%) | Qpq (%) | Qmu (%) | Qm nu (%) |
| 1 | T5 | Sublitharenite | 90.91 | 3.03 | 6.06 | 89.04 | 3.65 | 7.31 | 90.91 | 3.03 | 6.06 | 65.22 | 11.59 | 23.19 | 15.79 | 80.00 | 4.21 |
| 2 | T10 | Sublitharenite | 90.92 | 2.02 | 7.06 | 89.51 | 2.33 | 8.16 | 90.92 | 2.02 | 7.06 | 59.70 | 8.96 | 31.34 | 12.88 | 85.51 | 1.61 |
| 3 | T13 | Sublitharenite | 90.99 | 2.15 | 6.87 | 90.16 | 2.34 | 7.49 | 90.99 | 2.15 | 6.87 | 48.15 | 12.35 | 39.51 | 8.42 | 89.85 | 1.73 |
| 4 | T17 | Sublitharenite | 84.52 | 4.76 | 10.71 | 83.54 | 5.06 | 11.39 | 84.52 | 4.76 | 10.71 | 27.78 | 22.22 | 50.00 | 6.58 | 89.47 | 3.95 |
| 5 | T19 | Sublitharenite | 90.36 | 3.30 | 6.35 | 89.92 | 3.45 | 6.63 | 90.36 | 3.30 | 6.35 | 30.91 | 23.64 | 45.45 | 4.56 | 92.23 | 3.22 |
| 6 | T20 | Sublitharenite | 89.90 | 2.28 | 7.82 | 89.12 | 2.46 | 8.42 | 89.90 | 2.28 | 7.82 | 41.51 | 13.21 | 45.28 | 7.38 | 89.93 | 2.68 |
| 7 | T21 | Sublitharenite | 90.27 | 2.43 | 7.29 | 89.78 | 2.56 | 7.67 | 90.27 | 2.43 | 7.29 | 33.33 | 16.67 | 50.00 | 5.11 | 92.65 | 2.24 |
| 8 | T22 | Sublitharenite | 89.08 | 1.68 | 9.24 | 88.29 | 1.80 | 9.91 | 89.08 | 1.68 | 9.24 | 38.10 | 9.52 | 52.38 | 7.02 | 89.91 | 3.07 |
| 9 | T23 | Sublitharenite | 89.34 | 2.82 | 7.84 | 89.03 | 2.90 | 8.06 | 89.34 | 2.82 | 7.84 | 20.93 | 20.93 | 58.14 | 3.06 | 94.22 | 2.72 |
| 10 | T24 | Sublitharenite | 90.00 | 2.22 | 7.78 | 89.50 | 2.33 | 8.16 | 90.00 | 2.22 | 7.78 | 32.08 | 15.09 | 52.83 | 4.99 | 92.96 | 2.05 |
| **Max** | | | **90.99** | **4.76** | **10.71** | **90.16** | **5.06** | **11.39** | **90.99** | **4.76** | **10.71** | **65.22** | **23.64** | **58.14** | **15.79** | **94.22** | **4.21** |
| **Min** | | | **84.52** | **1.68** | **6.06** | **83.54** | **1.80** | **6.63** | **84.52** | **1.68** | **6.06** | **20.93** | **8.96** | **23.19** | **3.06** | **80.00** | **1.61** |
| **Average** | | | **89.32** | **2.76** | **7.82** | **88.47** | **2.98** | **8.44** | **89.32** | **2.76** | **7.82** | **40.32** | **15.56** | **44.12** | **7.89** | **89.25** | **2.77** |

Q=Total (Qm non+Qm un) and Qpq used for Folk (1980) classification (Qm+Qpq); F=Total feldspar grains (P+K); P=Plagioclase feldspar; K=Potassium feldspar; R=Total unstable rock fragments and chart used for Folk (1980) classification; Qm=Quartz monocrystalline Quartz; Qt=Total quartzose grains (Qm+Qp); Qpq=Polycrystalline quartz; Qmu=Undulose monocrystalline quartz; Qmnu=Non-Undulose monocrystalline quartz.

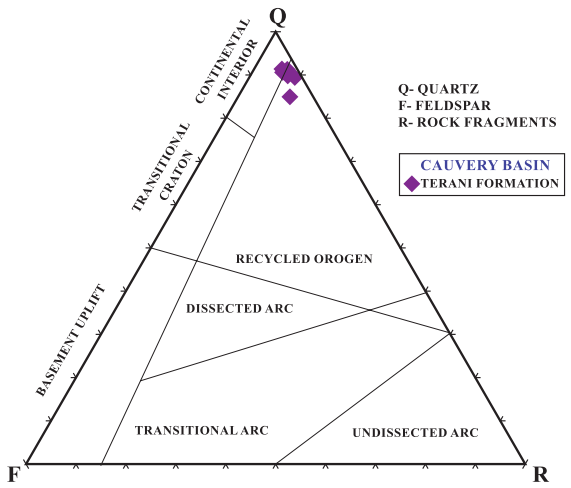


**Fig. 4.** Q–F–R Provenance discrimination diagram (Dickinson 1985) for the Terani sandstone (Q=Quartz, F=Feldspar and R=Rock fragments).

of the section, fine-grained quartz grains show dark encrustations, which could be organic carbon. There are many opaque grains along with feldspar grains as well. The cement is an argillaceous material. This petrographic type underwent shallow burial diagenesis. The alteration of feldspar increased to matrix cement.

## *Geochemistry*

### *Major element concentrations*

The Terani Formation consists of three types of lithology, which includes sandstone, clay, and calcrete. The concentrations of major oxides are listed in Table 3. In comparison with average UCC and PAAS values, sandstones are enriched in $SiO_2$ (~80.6–86 %) and $P_2O_5$ (~0.07–0.32 %) contents, while clay samples are enriched in $TiO_2$ (~0.55–1.4 %), $Al_2O_3$ (~14.41–33.6 %), $Fe_2O_3$ (~1.09–43 %), and $P_2O_5$ (~0.05–1.61 %) contents (Table 3). In the calcrete, enrichment of CaO is observed (~58.5–68 %), which is higher than the UCC and PAAS values. All oxides, except for CaO, are highly depleted in the calcrete samples in comparison to sandstone and clay. For comparison, MnO (~0.01–0.07 %), MgO (~0.06–0.98 %), CaO (~0.13–0.76 %), $Na_2O$ (~0.03–0.17 %), and $K_2O$ (~0.19–2.32 %) are enriched in sandstone and clay samples in comparison to calcrete (Table 3). The sandstone and clay show wide variations in $Na_2O$ and $K_2O$ contents. The $K_2O/Na_2O$ ratio is <1 in all samples, which indicates the predominance of plagioclase over k-feldspar.

### *Trace element concentrations*

The concentrations of trace elements are listed in Table 4. The trace elements are normalized to average UCC values (Taylor & McLennan 1985) and are plotted in the multi-elemental diagrams (Fig. 5).

### *Large ion lithophile elements (LILE)*

Among other trace elements, Rb, Ba, Sr, and Cs are considered LILE. The LILE elements are compared with UCC and PAAS in which Ba is higher in sandstones than in clay (Avg= 675 and 358 ppm, respectively). However, the average values of Rb, Sr, and Cs contents in sandstone (28, 229, and 0.2 ppm, respectively) and clay (19, 177, and 0.7 ppm, respectively) are depleted in comparison to UCC and PAAS. A positive correlation observed between Ba and Rb (r=0.70; number of samples, n=18) and also Rb with $K_2O$ (r=0.83) suggests that these elements are concentrated in clay phases (Armstrong-Altrin et al. 2017).

**Table 3:** Major element concentration in weight % for the Terani Formation – Cauvery Basin.

| Elements | Shale/Clay | | | | | | | | | | Avg. (n=11) | Sandstone | | | | Avg. (n=4) | Calcrete | | | Avg. (n=3) |
|---|---|---|---|---|---|---|---|---|---|---|---|---|---|---|---|---|---|---|---|---|
| | T1 | T2 | T3 | T4 | T6 | T8 | T11 | T12 | T14 | T16 | T18 | T5 | T10 | T13 | T17 | | T7 | T9 | T15 | |
| $SiO_2$ | 52.29 | 28.23 | 52.99 | 41.75 | 35.34 | 50.76 | 51.04 | 27.72 | 31.28 | 52.54 | 52.87 | 43.35 | 85.82 | 80.63 | 86.1 | 84.82 | 84.34 | 18.24 | 16.55 | 22.46 | 19.08 |
| $TiO_2$ | 1.34 | 0.55 | 1.29 | 1 | 0.83 | 1.33 | 1.22 | 0.64 | 0.74 | 1.41 | 1.14 | 1.04 | 0.07 | 0.48 | 0.18 | 0.23 | 0.24 | 0.56 | 0.44 | 0.85 | 0.62 |
| $Al_2O_3$ | 31.79 | 14.41 | 32.18 | 25.83 | 23.02 | 33.57 | 31.65 | 16.94 | 18.3 | 31.87 | 32.55 | 26.56 | 4.69 | 4.74 | 3.44 | 4.61 | 4.37 | 12.53 | 8.89 | 12.92 | 11.45 |
| $Fe_2O_3$ | 1.26 | 40.91 | 1.38 | 22.24 | 27.72 | 1.09 | 1.62 | 42.97 | 38.74 | 1.32 | 2.13 | 16.49 | 5.96 | 8.53 | 6.67 | 6.84 | 7 | 1.08 | 1.27 | 0.82 | 1.06 |
| MnO | 0 | 0 | 0 | 0 | 0.01 | 0.01 | 0.01 | 0.07 | 0.04 | 0.01 | 0 | 0.01 | 0.02 | 0 | 0.01 | 0.01 | 0.01 | 0 | 0.01 | 0.02 | 0.01 |
| MgO | 0.5 | 0.24 | 0.65 | 0.37 | 0.32 | 0.56 | 0.76 | 0.28 | 0.29 | 0.57 | 0.58 | 0.47 | 0.09 | 0.08 | 0.08 | 0.06 | 0.08 | 0.7 | 0.98 | 0.53 | 0.74 |
| CaO | 0.29 | 0.76 | 0.52 | 0.27 | 0.37 | 0.36 | 0.31 | 0.35 | 0.49 | 0.33 | 0.43 | 0.41 | 0.3 | 0.13 | 0.13 | 0.15 | 0.18 | 64.24 | 68.03 | 58.47 | 63.58 |
| $Na_2O$ | 0.11 | 0.11 | 0.1 | 0.07 | 0.05 | 0.06 | 0.08 | 0.05 | 0.08 | 0.04 | 0.08 | 0.08 | 0.12 | 0.17 | 0.1 | 0.14 | 0.13 | 0.04 | 0.04 | 0.03 | 0.04 |
| $K_2O$ | 1.02 | 0.75 | 1.17 | 0.99 | 0.52 | 0.56 | 0.66 | 0.47 | 0.52 | 1.06 | 1.03 | 0.8 | 1.5 | 2.32 | 1.08 | 1.18 | 1.52 | 0.25 | 0.19 | 0.39 | 0.28 |
| $P_2O_5$ | 0.09 | 1.61 | 0.81 | 0.25 | 0.2 | 0.05 | 0.06 | 0.28 | 0.12 | 0.07 | 0.06 | 0.33 | 0.11 | 0.32 | 0.07 | 0.09 | 0.15 | 0.04 | 0.04 | 0.04 | 0.04 |
| LOI | 10.62 | 11.92 | 8.17 | 6.66 | 10.69 | 10.61 | 11.86 | 9.61 | 8.2 | 9.83 | 9.06 | 9.75 | 1.27 | 1.98 | 1.39 | 1.04 | 1.42 | 1.74 | 2.73 | 2.99 | 2.49 |
| Total | 99.31 | 99.49 | 99.26 | 99.43 | 99.07 | 98.96 | 99.27 | 99.38 | 98.8 | 99.05 | 99.93 | 99.27 | 99.95 | 99.38 | 99.25 | 99.17 | 99.44 | 99.42 | 99.17 | 99.52 | 99.37 |
| $SiO_2/Al_2O_3$ | 1.64 | 1.96 | 1.65 | 1.62 | 1.54 | 1.51 | 1.61 | 1.64 | 1.71 | 1.65 | 1.62 | 1.65 | 18.3 | 17.01 | 25.03 | 18.4 | 19.68 | 1.46 | 1.86 | 1.74 | 1.69 |
| $K_2O/Al_2O_3$ | 0.03 | 0.05 | 0.04 | 0.04 | 0.02 | 0.02 | 0.02 | 0.03 | 0.03 | 0.03 | 0.03 | 0.03 | 0.32 | 0.49 | 0.31 | 0.26 | 0.34 | 0.02 | 0.02 | 0.03 | 0.02 |
| $K_2O/Na_2O$ | 9.27 | 6.82 | 11.7 | 14.14 | 10.4 | 9.33 | 8.25 | 9.4 | 6.5 | 26.5 | 12.88 | 11.38 | 12.5 | 13.65 | 10.8 | 8.43 | 11.34 | 6.25 | 4.75 | 13 | 8 |
| $Al_2O_3/TiO_2$ | 23.72 | 26.2 | 24.95 | 25.83 | 27.73 | 25.24 | 25.94 | 26.47 | 24.73 | 22.6 | 28.55 | 25.63 | 67 | 9.88 | 19.11 | 20.04 | 29.01 | 22.38 | 20.2 | 15.2 | 19.26 |
| $Al_2O_3/SiO_2$ | 0.61 | 0.51 | 0.61 | 0.62 | 0.65 | 0.66 | 0.62 | 0.61 | 0.59 | 0.61 | 0.62 | 0.61 | 0.05 | 0.06 | 0.04 | 0.05 | 0.05 | 0.69 | 0.54 | 0.58 | 0.6 |
| $Fe_2O_3+MgO$ | 1.76 | 41.15 | 2.03 | 22.61 | 28.04 | 1.65 | 2.38 | 43.25 | 39.03 | 1.89 | 2.71 | 16.95 | 6.05 | 8.61 | 6.75 | 6.9 | 7.08 | 1.78 | 2.25 | 1.35 | 1.79 |
| $K_2O+Al_2O_3$ | 32.81 | 15.16 | 33.35 | 26.82 | 23.54 | 34.13 | 32.31 | 17.41 | 18.82 | 32.93 | 33.58 | 27.35 | 6.19 | 7.06 | 4.52 | 5.79 | 5.89 | 12.78 | 9.08 | 13.31 | 11.72 |
| CIA | 96.11 | 93.55 | 95.74 | 95.61 | 97.27 | 96.38 | 97.4 | 96.63 | 96.34 | 96.33 | 96.31 | 96.15 | 72.03 | 63.3 | 72.06 | 75.36 | 70.69 | 97.39 | 97.04 | 96.48 | 96.97 |
| PIA | 99.41 | 98.69 | 99.47 | 99.54 | 99.64 | 98.05 | 99.58 | 99.5 | 99.26 | 99.79 | 99.58 | 99.32 | 93.95 | 90.41 | 93.25 | 93.54 | 92.79 | 99.47 | 99.25 | 99.61 | 99.44 |
| CIW | 99.43 | 98.76 | 99.49 | 99.56 | 99.64 | 98.09 | 99.59 | 99.52 | 99.29 | 99.79 | 99.6 | 99.34 | 95.96 | 95.25 | 95.44 | 95.24 | 95.47 | 99.48 | 99.27 | 99.62 | 99.45 |
| ICV | 0.14 | 3.01 | 0.16 | 0.97 | 1.3 | 0.12 | 0.15 | 2.65 | 2.23 | 0.15 | 0.17 | 1 | 1.72 | 2.47 | 2.4 | 1.87 | 2.11 | 5.34 | 7.98 | 4.73 | 6.02 |

CIA=$[Al_2O_3/(Al_2O_3+CaO^*+Na_2O+K_2O)]\times 100$ (Nesbitt & Young 1982). PIA=$100\times(Al_2O_3-K_2O)/(Al_2O_3+CaO^*+Na_2O-K_2O)$ (Fedo et al. 1995). ICV=$(Fe_2O_3+K_2O+Na_2O+CaO+MgO+MnO+TiO_2)/Al_2O_3$ (Cox et al. 1995).

*High field strength elements (HFSE)*

A significant depletion of HFSE is observed in the sandstone samples. Clay exhibits enrichment of Y (30 ppm), Th (15.25 ppm), and U (4 ppm), as well as depletion of Zr (109 ppm), Hf (3 ppm), and Nb (17 ppm) in comparison to UCC. A significant correlation is observed between Nb and $TiO_2$ (r=0.90, n=15) and reflects that these elements are most likely hosted by accessory phases, such as Ti-bearing minerals (Armstrong-Altrin et al. 2012). Similarly, a positive correlation observed between U and Ni (r=0.80, n=15) implies that these elements are associated with accessory phases (Ramos-Vázquez et al. 2017).

*Transitional trace elements (TTE)*

Co, Ni, Cr, and V are considered TTE. In the sandstones, average Ni (18 ppm), Cr (37 ppm) and V (33ppm) contents are depleted and the Co (25 ppm) content is slightly enriched in comparison to UCC (Fig. 5). However, the clay samples are enriched in Cr (138 ppm) and V (198 ppm) contents and depleted in Co (14 ppm) and Ni (51 ppm) contents, in comparison to average UCC values (Fig. 5). A significant correlation is observed between V and $TiO_2$ (r=0.62). The variation in trace element concentrations between the Terani sandstones and clay are most likely due to the influence of heavy minerals, as well as indicating the nature of source rocks.

*Rare earth element concentrations*

The REE concentrations of the Terani clastic rocks are given in Table 5. The REE contents are completely depleted in the sandstone and enriched in the shale samples when compared with UCC and PASS values. The total REE (ΣREE) content of the Terani clastic rocks vary from ~40 to 357 (Avg. 163). The chondrite normalized REE patterns show LREE enrichment and relatively flat HREE with a negative Eu anomaly ($Eu/Eu^*$ = ~0.02–0.49; Fig. 6). The average $Eu/Eu^*$ ratio of the Terani clastic rocks (0.15) are lower than the UCC (0.66) and PAAS (0.71). A positive correlation was observed between Y and ΣREE (r=0.61), as well as between ΣREE with $Al_2O_3$ (r=0.53). There is also a statistically significant (r=0.65) correlation

**Table 4:** Trace element concentrations in ppm for the Terani Formation – Cauvery Basin.

| Elements | Shale/Clay | | | | | | | | | | | Sandstone | | | | Avg. (n=4) | Calcrete | | | Avg (n=3) |
|---|---|---|---|---|---|---|---|---|---|---|---|---|---|---|---|---|---|---|---|---|
| | T1 | T2 | T3 | T4 | T6 | T8 | T11 | T12 | T14 | T16 | T18 | Avg. (n=11) | T5 | T10 | T13 | T17 | | T7 | T9 | T15 | |
| Sc | 13.91 | 14.21 | 12.68 | 17.84 | 15.25 | 13.03 | 12.42 | 13.27 | 17.02 | 16.16 | 16.24 | 14.73 | 2.39 | 9.75 | 3.6 | 6.52 | 5.57 | 0.71 | 0.54 | 0.65 | 0.64 |
| V | 162.71 | 215.02 | 160.52 | 230.54 | 214.45 | 157.29 | 158.96 | 223.49 | 213.3 | 218.87 | 217.05 | 197.47 | 31.51 | 37.27 | 30.3 | 34.54 | 33.4 | 16.3 | 16.89 | 15.95 | 16.38 |
| Cr | 145.01 | 116.89 | 139.94 | 120.08 | 199.64 | 128.96 | 140.39 | 102.05 | 119.36 | 189.01 | 116.11 | 137.95 | 20.09 | 68.71 | 23.77 | 34.55 | 36.78 | 15.73 | 15.09 | 12.1 | 14.31 |
| Co | 10.79 | 12.31 | 15.66 | 15.89 | 15.97 | 14.33 | 10.78 | 13.04 | 15.77 | 15.34 | 14.03 | 13.99 | 23.08 | 31.84 | 21.14 | 22.34 | 24.6 | 0.58 | 0.36 | 0.46 | 0.46 |
| Ni | 47.73 | 57.65 | 42 | 57.29 | 45.93 | 39.62 | 46.91 | 56.9 | 52.84 | 56.37 | 52.66 | 50.54 | 19.32 | 15.94 | 19.91 | 17.89 | 18.26 | 2.85 | 2.08 | 1.09 | 2.01 |
| Cu | 60.97 | 46.65 | 69.04 | 51.66 | 47.93 | 48.64 | 58.11 | 49.9 | 47.84 | 51.97 | 51.66 | 53.12 | 27.77 | 93.94 | 48.26 | 57.7 | 56.92 | 1.93 | 1.77 | 1.41 | 1.7 |
| Zn | 84.73 | 78.07 | 75.48 | 79.43 | 74.08 | 73.86 | 82.05 | 72.1 | 74.07 | 74.1 | 71.08 | 76.28 | 78.11 | 95.42 | 64.86 | 86.85 | 81.31 | 79.25 | 76.32 | 72.39 | 75.99 |
| Ga | 33.15 | 26.88 | 24.43 | 26.8 | 25.08 | 22.62 | 33.13 | 20.18 | 27.13 | 28.45 | 26.09 | 26.72 | 3.39 | 7.99 | 2.8 | 3.77 | 4.49 | 2.61 | 2.91 | 1.9 | 2.48 |
| Rb | 22.5 | 14.11 | 20.96 | 21.32 | 17.99 | 21 | 21.73 | 16.23 | 18.13 | 19.21 | 17.41 | 19.14 | 27.35 | 35.4 | 19.09 | 29.65 | 27.87 | 2.66 | 2.18 | 3.18 | 2.68 |
| Sr | 220.97 | 119.39 | 206.98 | 187.28 | 118 | 208.14 | 218.07 | 147.16 | 153.1 | 184.22 | 179.61 | 176.63 | 226.72 | 354.04 | 104.41 | 231.75 | 229.23 | 316.61 | 305.74 | 274.67 | 299.01 |
| Y | 63.58 | 12.33 | 68.34 | 13.72 | 13.65 | 56.06 | 56.22 | 12.84 | 10.43 | 13.4 | 10.62 | 30.11 | 3.94 | 27.18 | 6.41 | 7.89 | 11.35 | 101.76 | 117.64 | 127.57 | 115.66 |
| Zr | 148.45 | 91.39 | 138.84 | 94.33 | 90.16 | 137 | 134.41 | 93.94 | 91.1 | 92.36 | 91.5 | 109.41 | 57.56 | 224.06 | 157.91 | 87.54 | 131.77 | 24.61 | 23.67 | 30.38 | 26.22 |
| Nb | 21.25 | 13.93 | 20.68 | 16.42 | 12.51 | 21.69 | 20.62 | 15.09 | 14.91 | 15.03 | 15.74 | 17.08 | 1.08 | 6.55 | 2.56 | 1.33 | 2.88 | 10.95 | 9.92 | 11.18 | 10.68 |
| Cs | 0.73 | 0.71 | 0.65 | 0.88 | 0.54 | 0.73 | 0.78 | 0.74 | 0.66 | 0.86 | 0.59 | 0.72 | 0.31 | 0.2 | 0.17 | 0.18 | 0.22 | 0.09 | 0.04 | 0.04 | 0.06 |
| Ba | 304.55 | 432.08 | 303.49 | 496.23 | 434.57 | 312.57 | 312.71 | 414.07 | 436.4 | 486.22 | 451.31 | 398.56 | 698.58 | 740.52 | 637.36 | 621.65 | 674.52 | 53.42 | 57.76 | 51.37 | 54.18 |
| Hf | 4 | 2.82 | 3.71 | 2.75 | 2.36 | 3.97 | 3.99 | 1.58 | 1.83 | 2.66 | 2.71 | 2.94 | 1.85 | 11.77 | 4.54 | 2.84 | 5.25 | 0.39 | 0.42 | 0.74 | 0.52 |
| Ta | 1.17 | 1.01 | 0.96 | 1.06 | 1.14 | 1.09 | 1.76 | 1.05 | 1.2 | 1.05 | 1.06 | 1.14 | 0.06 | 0.39 | 0.15 | 0.53 | 0.28 | 0.01 | 0.09 | 0.02 | 0.04 |
| Pb | 16.32 | 9.33 | 12.83 | 9.58 | 8.62 | 14.3 | 14.71 | 8.35 | 9.31 | 9.54 | 9.13 | 11.09 | 12.25 | 13.71 | 12.54 | 10.69 | 12.3 | 1.79 | 1.24 | 1.59 | 1.54 |
| Th | 16.27 | 14.62 | 17.34 | 15.69 | 15.62 | 12.73 | 15.24 | 15.36 | 13.5 | 15.49 | 15.86 | 15.25 | 2.29 | 18.2 | 4.33 | 5.83 | 7.66 | 0.46 | 0.33 | 0.43 | 0.4 |
| U | 4.24 | 4.01 | 4.4 | 4.02 | 4.23 | 4.01 | 4.42 | 4.2 | 3.98 | 4 | 4.02 | 4.14 | 0.89 | 4.85 | 1.44 | 2.69 | 2.47 | 0.95 | 1.02 | 0.8 | 0.92 |
| Zr/Sc | 10.68 | 6.43 | 10.95 | 5.29 | 5.91 | 10.52 | 10.82 | 7.08 | 5.35 | 5.72 | 5.63 | 7.43 | 24.08 | 22.97 | 43.91 | 13.42 | 23.68 | 34.55 | 43.59 | 46.56 | 41.57 |
| Th/U | 3.84 | 3.65 | 3.94 | 3.9 | 3.7 | 3.17 | 3.45 | 3.65 | 3.39 | 3.87 | 3.95 | 3.68 | 2.58 | 3.75 | 2.99 | 2.16 | 3.1 | 0.48 | 0.32 | 0.54 | 0.44 |

between Y and ΣREE for the clastic rocks, suggesting the concentration of xenotime. However, the correlation between ΣREE and $Al_2O_3$ (r=0.06) is not significant and indicates the association of REE with accessory minerals.

## Discussion

### *Paleoweathering*

The sandstones predominantly contain monocrystalline, as well as polycrystalline quartz grains with undulose extinction. A low percentage of rock fragments followed by feldspar in sandstones suggests that they had been derived from igneous and metamorphic rocks with high intensity of chemical weathering rather than physical weathering under humid climatic conditions (Basu 2020; Jamwal et al. 2020). In comparison with North American Shale Composite, the $K_2O/Na_2O$ ratio is higher (11) in the Terrani clastic rocks (NASC=3.5), which indicates the likely destruction of plagioclase in the source area. The $K_2O/Al_2O_3$ ratio is widely used to infer the composition of terrigenous rocks, since the ratio values are different for clay minerals and feldspars. Cox et al. (1995) suggested that the ratio for clay is <0.30, while it varies for feldspars from ~0.30 to 0.90. The low values of the $K_2O/Al_2O_3$ ratio (0.11) suggest a strong influence of clay minerals, particularly kaolinite, which may be the $Al_2O_3$ and $K_2O$ bearing mineral in the Terani clastic rocks. A strong positive correlation between $Al_2O_3$ and $TiO_2$ (r=0.97; n=15) indicates the association of Ti with phyllosilicates, such as illite and kaolinite (Paikaray et al. 2008). However, Rb, Ba, and Cs exhibit a positive correlation with $Al_2O_3$ (r=0.012, 0.38 and 0.78, respectively), suggesting its association with clay minerals, i.e., kaolinite and montmorillonite (Ramos-Vázquez & Armstrong-Altrin 2019).

The weathering intensity in the source area can be estimated through weathering indices such as the Chemical Index of Alteration (CIA: Nesbitt & Young 1982), the Chemical Index of Weathering (CIW: Harnois 1988) and the Plagioclase Index of Alteration (PIA: Fedo et al. 1995). Recently, weathering indices have been extensively used by numerous researchers to infer the intensity of weathering (Veena et al. 2014; Bandopadhyay & Ghosh 2015; Armstrong-Altrin et al. 2015; Ramos-Vázquez et al. 2017; Mude et al. 2020). The influence of chemical weathering may affect the mineralogy and major element composition of sediments by the removal of labile cations such as $Ca^{2+}$, $Na^{+}$, and $K^{+}$ that are relative to residual

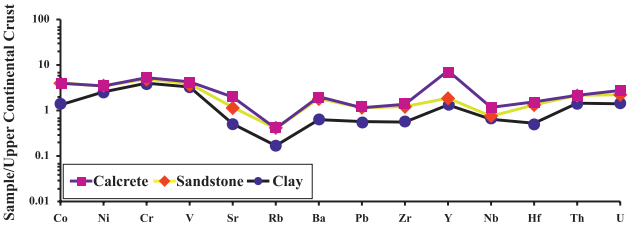


**Fig. 5.** Average Upper Continental Crust (UCC; Taylor & McLennan 1985) normalized trace element plot of the Terani Formation, Cauvery Basin.

constituents ($Al^{3+}$ and $Ti^{4+}$) through the conversion of feldspar to clay minerals (Nesbitt & Young 1982).

The CIA index (Nesbitt & Young 1982) helps to estimate the degree of weathering of rocks, with higher values (>70) suggesting greater alteration, which can be estimated using molar proportions:

$$CIA=[Al_2O_3/(Al_2O_3+CaO^*+Na_2O+K_2O)]\times 100, \quad (1)$$

where $CaO^*$ represents the amount of CaO incorporated in silicate phases. If the CIA value is <50, which represents an unweathered product, values between 50 and 70 indicate little weathering, while values between 70 and 80 refer to moderate weathering, and values >80 refer to intense weathering. The CIA values of the Terani Formation (62–97; Avg. 88; Table 3) suggest moderate to intense weathering, thus reflecting hot and humid climatic conditions with high kaolinite and low illite contents in the source area.

With regards to the degree of weathering, the CIA is insensitive when it is reintroduced into the system. Therefore, Harnois (1988) proposed another index called the Chemical Index of Weathering.

$$CIW=[Al_2O_3/(Al_2O_3+CaO^*+Na_2O)]\times 100 \quad (2)$$

This index is not applicable for post depositional K enriched sediments and is based on the presumption that Al remains in the system and accumulates in the residue while Na and Ca leached away. The CIW values of Terani clastic rocks (~98) are higher than those of the UCC and PAAS values, thereby denoting intense weathering in the source area.

Fedo et al. (1995) proposed an index to measure the chemical weathering of source rocks named the Plagioclase Index of Alteration (PIA).

$$PIA=[(Al_2O_3-K_2O)/(Al_2O_3+Na_2O+CaO^*-K_2O)]\times 100 \quad (3)$$

The average PIA value in the Terani clastic rocks is ~97 (Table 3), which confirms the possibility for the high intensity of chemical weathering, and also reveals the conversion of plagioclase to clay minerals (Mongelli et al. 2006).

The ratio of Th/U is extensively used to study the source rock characteristics of sedimentary rocks (e.g., Roddaz et al. 2006; Tapia-Fernandez et al. 2017; Ayala-Pérez et al. 2021). The sediments exhibit higher Th/U ratios, which are largely due to oxidative weathering and removal of U in highly-weathered source rocks (McLennan et al. 1980). The clastic sedimentary rocks derived from the upper crust are characterized by a Th/U ratio equal to or greater than 4, whereas a Th/U ratio lower than 4 is related to mantle contribution (McLennan et al. 1980). The Th/U ratio in the Terani clastic rocks are less than 4 (3.9), thus suggesting mantle derivation or intense weathering in the source area.

### *Provenance*

Paleogeographically, the sandstones of the Terani Formations are fluviatile to paralic. The sandstones are dominated by bedding, which is considered to represent bank fluvial and lacustrine deposits; however, they are not diagnostic. The presence of a small amount of glauconite in the sandstones' interbeds, as well as in the in-fillings of the burrows in the studied samples, indicate a connection with marine environments that is suggestive of tidal influence in the area, i.e., paralic conditions. The fine laminations in the sandstones point towards lower energy conditions and lower sedimentation rates. The structure of fewer sandstones, which occurs intermittently, shows a sporadic high energy condition. The above-mentioned features confirm a fluviatile or paralic environment of deposition of the Terani Formation. Lithic fragments are abundant in the Terani sandstones, which are derived from the nearby igneous, metamorphic, and sedimentary source rocks. In Figure 4, the trend of the samples suggests that the Cauvery Basin received its debris from orogenic sources. The domination of lithic fragments of metamorphic, igneous, and sedimentary rocks, as well as an abundance of monocrystalline quartz with low undulosity (≤5°) in the Terani sandstones, further corroborates with the Archaean group of rocks as potential source rocks. The plagioclase grains with both Carlsbad twinning and albitic twinning in the Terani sandstone support a detrital rather than an authigenic origin (Middleton 1972; Scarciglia et al. 2016). Relatively high proportions of monocrystalline quartz in the sandstone may be attributed to the disaggregation of original polycrystalline quartz during high energy and/or long-distance transport from the source area. The polycrystalline quartz grains exhibit straight to slightly curved intercrystalline boundaries, which suggests that the Terani sandstone was derived from plutonic igneous rocks. In addition, undulose extinction in some grains is related to a low degree of metamorphic source rocks (Folk 1980). In comparison to the plagioclase feldspars, the alkali feldspars are slightly enriched, which further supports a granitic source.

The ultrastable minerals (zircon, tourmaline and rutile) possess euhedral, pyramidal, and sub-rounded grains with sharp boundaries, which suggest their derivation from metamorphic and acidic, igneous source rocks (Imchen et al. 2014; Subin Prakash et al. 2018; Hossain et al. 2020; Ramos-Vázquez & Armstrong-Altrin 2020; Karlik et al. 2021). The high content of ilmenite grains in the Terani sandstones are often derived from the granitic rocks of the Dharwar Craton (Subin Prakash et al. 2018). The metastable garnet, which is accompanied by staurolite, sillimanite, and kyanite, suggests a significant

**Table 5:** Rare earth element concentrations (ppm) for the Terani Formation – Cauvery Basin.

| Elements | Shale/Clay | | | | | | | | | | Avg. (n=11) | Sandstone | | | | Avg. (n=4) | Calcrete | | | Avg. (n=3) |
|---|---|---|---|---|---|---|---|---|---|---|---|---|---|---|---|---|---|---|---|---|
| | T1 | T2 | T3 | T4 | T6 | T8 | T11 | T12 | T14 | T16 | T18 | T5 | T10 | T13 | T17 | | T7 | T9 | T15 | |
| La | 75.51 | 29.2 | 70.65 | 26.27 | 21.61 | 67.98 | 68.21 | 21.33 | 29.73 | 24.13 | 21.12 | 41.43 | 12.96 | 33.76 | 7.5 | 32.68 | 21.72 | 35.15 | 30.88 | 38.93 | 34.99 |
| Ce | 122.43 | 25.15 | 116.1 | 29.47 | 27.28 | 122.58 | 112.32 | 24.29 | 28.39 | 27.87 | 27.44 | 60.3 | 31.13 | 34.18 | 16.42 | 24.9 | 26.66 | 18.37 | 19.89 | 17.44 | 18.57 |
| Pr | 18.29 | 4.81 | 17.92 | 4.62 | 5.08 | 18.28 | 16.72 | 3.39 | 4.48 | 4.6 | 4.01 | 9.29 | 3.2 | 12.69 | 1.95 | 7.57 | 6.35 | 10.12 | 11.78 | 13.12 | 11.67 |
| Nd | 71.51 | 12.22 | 70.6 | 15.46 | 14.22 | 71.41 | 71.6 | 15.99 | 12.14 | 15.08 | 15.21 | 35.04 | 9.62 | 24.88 | 7.38 | 18.56 | 15.11 | 69.28 | 66.23 | 65.62 | 67.04 |
| Sm | 16.06 | 3.29 | 13.93 | 3.09 | 2.8 | 15.75 | 16.61 | 2.53 | 3.46 | 3.07 | 3.32 | 7.63 | 1.37 | 7.41 | 1.58 | 5.79 | 4.04 | 15.32 | 14.39 | 11.23 | 13.65 |
| Eu | 4.01 | 0.89 | 2.86 | 0.81 | 0.23 | 3.32 | 4.05 | 1.3 | 1.28 | 0.78 | 0.46 | 1.82 | 0.44 | 1.69 | 0.45 | 0.57 | 0.79 | 4.45 | 5.37 | 5.46 | 5.09 |
| Gd | 15.26 | 2.7 | 13.93 | 2.97 | 1.41 | 15.93 | 14.49 | 2.03 | 2.14 | 2.87 | 1.34 | 6.82 | 1.06 | 6.4 | 1.37 | 4.78 | 3.4 | 16.11 | 10.74 | 12.66 | 13.17 |
| Tb | 2.5 | 0.95 | 2.47 | 0.53 | 1.06 | 1.71 | 2.39 | 0.78 | 0.83 | 0.51 | 0.97 | 1.34 | 0.18 | 1.04 | 0.25 | 0.16 | 0.41 | 2.16 | 2.74 | 2.36 | 2.42 |
| Dy | 13.11 | 2.46 | 11.72 | 2.88 | 2.51 | 13.74 | 13.38 | 1.86 | 1.65 | 2.83 | 1.87 | 6.18 | 0.93 | 5.36 | 1.41 | 1.52 | 2.3 | 12.63 | 12.68 | 9.61 | 11.64 |
| Ho | 2.84 | 1.12 | 1.11 | 0.69 | 0.23 | 1.68 | 2.43 | 0.61 | 0.95 | 0.68 | 1.01 | 1.21 | 0.21 | 1.19 | 0.33 | 0.49 | 0.55 | 2.93 | 2.58 | 1.99 | 2.5 |
| Er | 7.34 | 1.07 | 5.19 | 1.96 | 1.64 | 6.09 | 5.71 | 0.7 | 1.02 | 1.95 | 0.13 | 2.98 | 0.59 | 3.22 | 0.94 | 1.09 | 1.46 | 6.4 | 4.27 | 3.24 | 4.63 |
| Tm | 1.08 | 0.11 | 0.87 | 0.29 | 0.18 | 1.27 | 1.61 | 0.22 | 0.15 | 0.28 | 0.19 | 0.57 | 0.09 | 0.46 | 0.13 | 0.1 | 0.2 | 0.86 | 1.09 | 0.76 | 0.9 |
| Yb | 6.2 | 1.64 | 5.45 | 1.85 | 1.17 | 4.85 | 5.81 | 1.35 | 1.3 | 1.69 | 1.67 | 3 | 0.54 | 2.88 | 0.9 | 0.94 | 1.31 | 5.5 | 4.26 | 5.25 | 5 |
| Lu | 0.96 | 0.01 | 0.54 | 0.3 | 0.26 | 0.76 | 0.88 | 0.27 | 0.23 | 0.28 | 0.25 | 0.43 | 0.08 | 0.45 | 0.14 | 0.28 | 0.24 | 0.83 | 0.57 | 0.76 | 0.72 |
| ΣREE | 357.11 | 85.62 | 333.33 | 91.19 | 79.7 | 345.37 | 336.22 | 76.65 | 87.77 | 86.61 | 78.96 | 178.05 | 62.41 | 135.6 | 40.74 | 99.43 | 84.55 | 200.11 | 187.47 | 188.45 | 192.01 |
| LREE | 303.8 | 74.66 | 289.2 | 78.92 | 71 | 296.01 | 285.47 | 67.53 | 78.21 | 74.74 | 71.09 | 153.69 | 58.28 | 112.92 | 34.83 | 89.49 | 73.88 | 148.25 | 143.17 | 146.35 | 145.92 |
| HREE | 34.04 | 7.36 | 27.34 | 8.5 | 7.06 | 30.11 | 32.21 | 5.78 | 6.14 | 8.22 | 6.08 | 15.71 | 2.63 | 14.6 | 4.1 | 4.59 | 6.48 | 31.3 | 28.18 | 23.98 | 27.82 |
| LREE/HREE | 8.93 | 10.15 | 10.58 | 9.29 | 10.06 | 9.83 | 8.86 | 11.69 | 12.74 | 9.09 | 11.7 | 10.26 | 22.16 | 7.74 | 8.5 | 19.5 | 14.47 | 4.74 | 5.08 | 6.1 | 5.31 |
| Eu/Eu* | 0.03 | 0.16 | 0.02 | 0.14 | 0.1 | 0.02 | 0.03 | 0.41 | 0.28 | 0.14 | 0.17 | 0.14 | 0.49 | 0.06 | 0.34 | 0.03 | 0.23 | 0.03 | 0.06 | 0.06 | 0.05 |
| (La/Yb)cn | 8.23 | 12.06 | 8.76 | 9.62 | 12.5 | 9.46 | 7.93 | 10.68 | 15.4 | 9.67 | 8.53 | 10.26 | 16.14 | 7.93 | 5.66 | 23.5 | 13.31 | 4.32 | 4.9 | 5.01 | 4.74 |
| (La/Sm)cn | 2.96 | 5.59 | 3.19 | 5.35 | 4.85 | 2.72 | 2.58 | 5.31 | 5.4 | 4.95 | 4.01 | 4.27 | 5.94 | 2.87 | 2.98 | 3.55 | 3.84 | 1.44 | 1.35 | 2.18 | 1.66 |
| (Gd/Yb)cn | 1.99 | 1.34 | 2.07 | 1.3 | 0.98 | 2.66 | 2.02 | 1.22 | 1.33 | 1.38 | 0.65 | 1.54 | 1.59 | 1.8 | 1.24 | 4.13 | 2.19 | 2.38 | 2.04 | 1.95 | 2.12 |
| (La/Lu)cn | 8.16 | 244.21 | 13.53 | 9.12 | 8.6 | 9.25 | 8.08 | 8.21 | 13.3 | 8.94 | 8.94 | 30.94 | 16.21 | 7.74 | 5.4 | 11.93 | 10.32 | 4.41 | 5.59 | 5.3 | 5.1 |
| La/Th | 4.64 | 2 | 4.08 | 1.67 | 1.38 | 5.34 | 4.48 | 1.39 | 2.2 | 1.56 | 1.33 | 2.73 | 5.66 | 1.85 | 1.73 | 5.6 | 3.71 | 76.96 | 94.9 | 91.14 | 87.67 |

Eu/Eu* =EuCN/[(SmCN)*(GdCN)]1/2. CN = chondrite normalized (Taylor and McLennan, 1985). LREE = La, Ce, Pr, Nd, and Pm; HREE = Tb, Dy, Ho, Er, Tm, Yb, and Lu. Avg.=Average.

contribution of medium to high grade metamorphic rocks (Morton et al. 2005).

The concentration of major, trace, and rare earth elements in clastic sediments can provide reliable information about the source area, and numerous researchers have previously utilised the sediment composition to infer provenance (Nagarajan et al. 2015; Tanner & Lucas 2017; Yang & Du 2017; Maftei et al. 2019; Al-Jaberi & Al-Jafar 2020; Cusack et al. 2020; George-Marian et al. 2020). Among other trace elements, REE and HFSE, such as Zr, Hf, Y, and Nb are particularly useful because of their low mobility during weathering and transportation, as well as diagenetic process (Cullers 2000). Furthermore, the REE pattern and relative size of the Eu anomaly have been used to decipher the nature of the source rocks (Cullers 1994; Zhang & Gao 2015; Hernández-Hinojosa et al. 2018; Anaya-Gregorio et al. 2018; Armstrong-Altrin et al. 2018).

The enrichment of $Al_2O_3$, $Fe_2O_3$, CaO, and $P_2O_5$, as well as depletion of $SiO_2$, $TiO_2$, MnO, MgO, $Na_2O$, and $K_2O$ relative to UCC in the Terani clastic rocks may be due to their derivation by a combination of various sources. Among major oxides, $Al_2O_3$ and $TiO_2$ are immobile during weathering, transportation, and diagenesis, and hence the $Al_2O_3/TiO_2$ ratio is widely used to infer the source rock composition (Zhou et al. 2015; Kettanah et al. 2020). The ratio of $Al_2O_3/TiO_2$ varies from 3 to 8 for mafic, ~8 to 21 for intermediate, and ~ 21 to 70 for felsic igneous rocks (Hayashi et al. 1997). A wide variation in the $Al_2O_3/TiO_2$ ratio (~10–67) reveals the combination of intermediate and felsic source rocks. The average $Fe_2O_3$ content in the Terani clastic rocks is 12.8 %, which is slightly higher than the UCC, indicating that the detritus was derived from the Fe rich source rocks.

During the magmatic process, the ferromagnesium elements, such as Cr, Ni, Co, and V show similarities in their behaviours, however, they may be fractionated during weathering (Feng & Kerrich 1990). A high content of these elements in clastic sediments are indicative of mafic provenance (Armstrong-Altrin et al. 2004; Hu et al. 2017; Alexandrowicz 2019: Damian et al. 2019; Bessa et al. 2020; Li et al. 2020). In the Terani Formation, Ni is depleted, whereas Cr is enriched in all of the samples with respect to the average UCC composition.

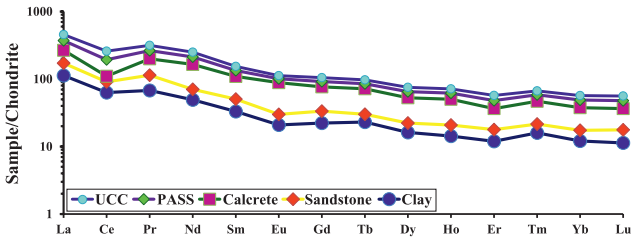


**Fig. 6.** Average Chondrite normalized rare earth element plots for the Terani sandstones and Upper Continental Crust (UCC) values of Taylor & McLennan (1985).

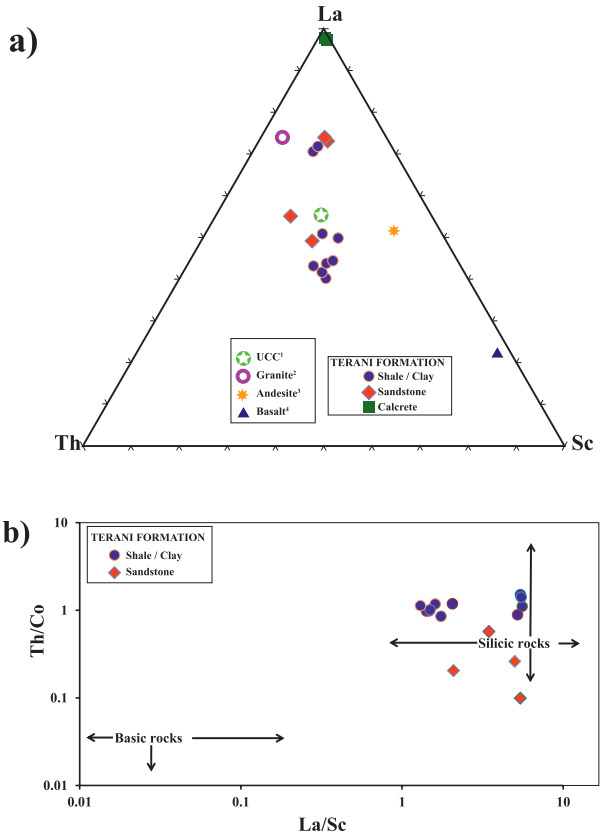


**Fig. 7. a** — La–Th–Sc ternary diagram for the Terani clastic rocks ([1]Taylor & McLennan 1985 and [2,3,4]Condie 1993). **b** — Th/Co versus La/Sc plot to infer source rock types for the Terani clastic rocks (Fields after Cullers 2002).

The depletion of Ni in the studied samples implies input of detritus from felsic source terrain. Moreover, enrichment of Cr in the Terani clastic rocks (95 ppm) and the Cr/Ni ratio (2.10) suggest that the presence of detritus was derived from a felsic source rather than an ultramafic source. Furthermore, a significant correlation is observed for Cr with Ni (r=0.85), and Ni with Co (r=0.21) suggests significant contribution from felsic rocks (Asiedu et al. 2000). In this study, we assume that the depletion of Ni accompanied by Cr is probably due to the concentration of garnet in sandstones, which was derived from felsic source rocks, and did not represent the mafic nature of source rocks. Garver et al. (1996) suggested that high Cr and Ni abundance (Cr >150 ppm and Ni >100 ppm) in the clastic sediments is an indication of ultramafic rocks in the source area. The Terani clastic rocks have depleted values of Cr (95 ppm) and Ni (35 ppm), thus indicating the absence of ultramafic rocks in the source area as well.

Many researchers have used the ratio of Th and La (indicative of felsic), as well as Sc and Co (indicative of mafic) to differentiate felsic and mafic provenances (McLennan et al. 1980; Cullers 2002; Kasanzu et al. 2008; Armstrong-Altrin et al. 2019, 2020). The ternary plots of La–Th–Sc and a bivariate plot of Th/Co vs. La/Sc can provide valuable information regarding the source rock characteristics (Cullers 2002). In the La–Th–Sc ternary diagram (Fig. 7a), the average composition of granite, andesite, and basalt (Condie 1993), and UCC value are used in this plot for comparison. In this diagram, the samples are plotted near the granite and the UCC composition, which suggests that the Terani clastic rocks were derived by the influence of felsic and intermediate source rocks. Similarly, the plot of Th/Co vs La/Sc (Fig. 7b) also suggests a felsic nature of the source rocks (Cullers 2002).

The average Zr content (100.5) and Zr/Hf ratio (34.9) in the Terani clastic rocks is slightly lower than the average UCC value (~193 and ~36, respectively; Rudnick & Gao 2003). The Zr content does not show any distinct correlation with HREE, thereby suggesting that HREEs are not controlled by zircon abundance. The ratios of Zr/Sc and Th/Sc are considered powerful provenance indicators (Cullers 2002). The Th/Sc ratio is a useful index of fractionation of magmatic rocks because Th is an incompatible element, while Sc is typically compatible during magmatic differentiation. The Zr/Sc ratio is a useful index of zircon enrichment, because Zr is strongly enriched in zircon and Sc preserves the signature of source rocks. According to Taylor & McLennan (1985), the Th/Sc ratios are reliable indicators of provenance, and these elements are not contained in minerals that are easily fractionated during the sedimentation process. The Th/Sc ratios of Terani clastic rocks are >1 (1.9), suggesting an inclination towards felsic sources. In addition, sorting and recycling processes during transportation would result an increase of Zr/Sc ratio value.

In clastic sedimentary rocks, a higher LREE/HREE ratio and negative Eu anomaly are characteristic of felsic rocks. However, sediments sourced from mafic rocks have a low LREE/HREE ratio and a positive Eu anomaly (Cullers 1994). In this study, the clastic rocks exhibit a high LREE/HREE ratio with a negative Eu anomaly, implying that the detritus was derived from felsic and intermediate source rocks (Cullers 2002).

The ΣREE concentration of the Terani sediments (~192.01) and Dharwar Cratons of Granite (~261.97, Jayananda et al. 1995) and Gneisses (~265.85) are higher than the UCC (~148.14) and PAAS (~184.77) values. In order to determine the probable source rocks for the Terani clastic rocks, the average REE patterns are compared with those of charnockites and gneisses from the Kerala Khondalite Belt (Allen et al.

1985; Chacko et al. 1992) and Dharwar Craton (Jayananda et al. 1995; Stähle et al. 1987) (Fig. 8). These areas are relatively close to the Terani Formation and are assumed to contribute sediments to the study area. The chondrite normalized REE patterns of the Terani clastic rocks are LREE enriched and flat HREE with a significant Eu anomaly. The REE pattern and the size of the Eu anomaly are very similar to the gneisses of the Dharwar Craton (Fig. 8). This comparison suggests that the study area received a higher contribution of sediments from the Dharwar Craton rather than the Kerala Khondalite belt.

During the Phanerozoic Eons, granitic rocks are abundant in K-feldspar, thereby reflecting less depletion of Eu and high depletion of HREE with $(Gd/Yb)_{cn}$ ratio <2 (McLennan et al. 1993). On the $Eu/Eu^*$ vs $(Gd/Yb)_{cn}$ plot (Fig. 9), few samples plot in the field of Phanerozoic (K-feldspar rich granites reflect less depletion of Eu), which shows $Gd_{cn}/Yb_{cn}$ ratio <2.0, whereas few samples show $Gd_{cn}$/Ybcn ratio >2.0 and low $Eu/Eu^*$ ratio. However, the studied sandstone and clay show low $Eu/Eu^*$ and high $Gd_{cn}/Yb_{cn}$ ratio <2, which suggests an Archaean igneous source.

The ratios of $Eu/Eu^*$, $(La/Lu)_{cn}$, La/Sc, La/Co, Th/Sc, Th/Co and Cr/Th are widely used to interpret the composition of the source rocks, since REE, Th, and La abundances are higher in felsic rocks than in basic rocks, whereas the Co, Sc, and Cr contents are higher in mafic rocks than in felsic rocks (Cullers 1994, 2000, 2002; Armstrong-Altrin et al. 2004; Tijani et al. 2010; Hu et al. 2017). These ratios of the studied Terani clastic rocks are compared with those of the possible source rocks, UCC, and with sediments derived from mafic and felsic rocks (Table 6). The $Eu/Eu^*$, $(La/Lu)_{cn}$, La/Sc, La/Co, Th/Sc, Th/Co, and Cr/Th ratios of the Terani Formation fall within the range of sediments derived from felsic to intermediate source rocks.

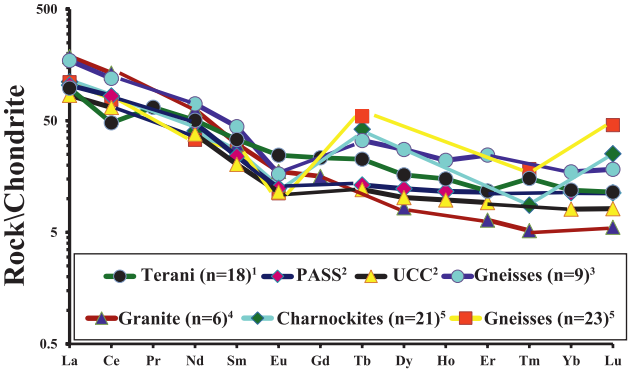


**Fig. 8.** Chondrite-normalized REE patterns. N=number of samples; [1]This study (Terani Formations); [2]average UCC and PAAS (Taylor & McLennan 1985); [3]Dharwar Craton (Stähle et al. 1987); [4]Dharwar Craton (Jayananda et al. 1995); [5]Kerala Khondalite Belt (Allen et al. 1985; Chacko et al. 1992).

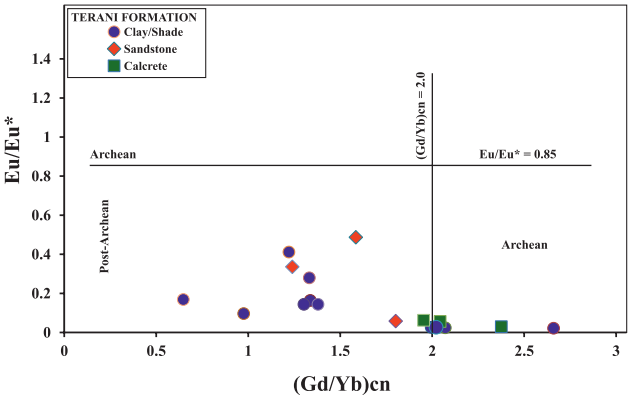


**Fig. 9.** Plot of $Eu/Eu^*$ vs $(Gd/Yb)_{CN}$ for Terani clastic rocks of the Cauvery Basin, fields according to McLennan & Taylor (1991).

### *Tectonic setting*

The petrography study reveals that the studied sediments are characterized by (a) higher proportion of quartz, (b) predominance of monocrystalline grains, (c) feldspar affinity, (d) highly albitic plagioclase grains, and (e) low F/R ratio (0.35 %). These properties are consistent with those of clastic rocks that were deposited in a passive continental margin environment (Taylor & McLennan 1985).

In clastic sediments, the major element-based discrimination diagrams of Bhatia (1983) and Roser & Korsch (1986) have been traditionally used in various studies to infer the tectonic settings of unknown basins (Tobia & Aswad 2015; Ma et al. 2018; Zaid et al. 2018; Bessa et al. 2021). Recently, however, Verma & Armstrong-Altrin (2013, 2016) evaluated these old discrimination diagrams and interpreted the inconsistencies when applying these diagrams to identify the tectonic setting of a sedimentary basin. On the basis of the major and trace element concentrations of clastic sediments, these authors further proposed a statistically-based discriminant function diagram to infer the tectonic setting of unknown sedimentary basins. In order to infer the probable tectonic setting of the Terani Formation, we applied the recently proposed discriminant-function diagram of Verma & Armstrong-Altrin (2016), which is capable of discriminating the sediments derived from passive and active margin settings. On these discrimination diagrams, all except for four samples, the Terani clastic rocks are plotted exclusively in the passive margin field (Fig. 10a and b).

## Conclusions

The Terani Formation represents the syn-rift Lower Cretaceous sequences exposed in the Cauvery Basin dominated by bedded, fine-grained siliclastic deposits of fluviatile to paralic and lacustrine deposits. Texturally, the Terani sandstones are sub-angular to sub-rounded and moderately-sorted to well-sorted lithic dominated arenites. The predominance of monocrystalline quartz with straight to slightly curved intercrystalline boundaries, abundance of lithic fragments (Q89–F3–R8), and low F/R ratio (0.35 %) are consistent with those of sediments derived from igneous and metamorphic rocks

**Table 6:** Range of elemental ratios of sediments in this study compared to the ratios in similar fractions derived from felsic and mafic rocks.

| Elememtal Ratio | Range of sediments from Cauvery Basin TERANI FORMATION[1] | Range of sediments from felsic sources[2] | Range of sediments from mafic sources[2] | Upper continental Crust [3] | Post Archean Australian Average Shale[3] |
|---|---|---|---|---|---|
| Eu/Eu* | 0.02–0.49 | 0.40–0.94 | 0.71–0.95 | 0.63 | 0.66 |
| (La/Lu)cn | 0.18–59.02 | 3.00–27.00 | 1.10–7.00 | 9.73 | 9.17 |
| La/Sc | 1.30–59.67 | 2.5–16.3 | 0.43–0.86 | 2.21 | 2.4 |
| Th/Sc | 0.60–1.87 | 0.84–20.5 | 0.05–0.02 | 0.79 | 0.9 |
| Th/Co | 0.10–1.51 | 0.67–19.4 | 0.04–1.4 | 0.63 | 0.63 |
| Th/Cr | 0.02–0.26 | 0.13–2.7 | 0.018–0.046 | 0.13 | 0.13 |
| Cr/Th | 3.77–46.39 | 4.00–15.0 | 25–500 | 7.76 | 7.53 |
| La/Co | 0.35–86.90 | 1.80–13.8 | 0.14–0.38 | 1.76 | 1.65 |

[1] This study; [2] Cullers (1994, 2000); Cullers & Podkovyrov (2000); Cullers et al. (1988); Armstrong–Altrin (2009); [3] McLennan (2001); Taylor & McLennan (1985).

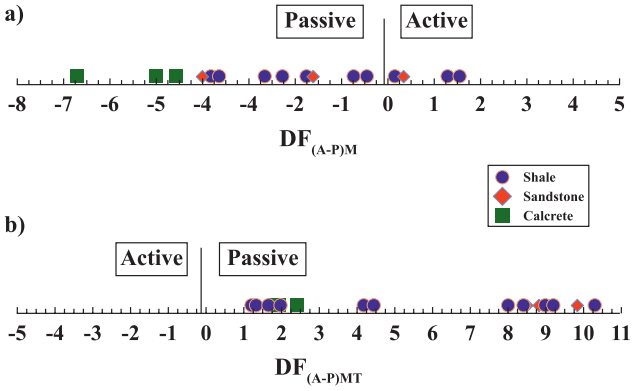


**Fig. 10. a** — Major element (M) based diagram for the discrimination of active (AM) and passive (PM) margin settings (Verma & Armstrong-Altrin 2016). The function ($DF_{(AP)M}$) is derived from the equation: $DF_{(AP)M}=(3.0005\times ilr1_{TiM})+(-2.8243\times ilr2_{AlM})+(-1.0596\times ilr3_{FeM})+(-0.7056\times ilr4_{MnM})+(-0.3044\times ilr5_{MgM})+(0.6277\times ilr6_{CaM})+(-1.1838\times ilr7_{NaM})+(1.5915\times ilr8_{KM})+(0.1526\times ilr9_{PM})-5.9948$. ilr=isometric log-ratio transformation. **b** — Major and trace elements (MT) based diagram for the discrimination of active (A) and passive (P) margin settings (Verma & Armstrong-Altrin 2016). The function ($DF_{(AP)MT}$) is calculated from the equation: $DF_{(AP)\,MT}=(3.2683\times ilr1_{TiMT})+(5.3873\times ilr2_{AlMT})+(1.5546\times ilr3_{FeMT})+(3.2166\times ilr4_{MnMT})+(4.7542\times ilr5_{MgMT})+(2.0390\times ilr6_{CaMT})+(4.0490\times ilr7_{NaMT})+(3.1505\times ilr8_{KMT})+(2.3688\times ilr9_{PMT})+(2.8354\times ilr10_{CrMT})+(0.9011\times ilr11_{NbMT})+(1.9128\times ilr12_{NiMT})+(2.9094\times ilr13_{VMT})+(4.1507\times ilr14_{YMT})+(3.4871\times ilr15_{ZrMT})-3.2088$. ilr = isometric log–ratio transformation.

with high intensity of chemical weathering under humid climatic conditions in a passive continental margin. The geochemical study on the samples of the Terani Formation has provided reliable information on the paleoweathering, tectonic setting, and provenance characteristics. The samples of the Terani Formation show higher CIA, PIA, CIW, and $K_2O/Na_2O$ ratios, and the A–CN–K diagram demonstrates that the Terani clastic rocks were derived from high to moderately-weathered source rocks. The $Al_2O_3/TiO_2$, La/Sc, Th/Sc, and Cr/Th ratios revealed a heterogeneous provenance, which varies from felsic to intermediate source rocks.

The Chondrite normalized REE pattern implies significant LREE enrichment, HREE depletion, and negative Eu anomalies. The samples provide wide variation in ΣREE contents, as well as La and Ce concentrations, and such variations are either due to grain size effect or inclusions of monazite. The observed strong positive correlation between La and Ce (r=0.92) indicate that the inclusions of heavy minerals in them produced abnormal contents of rare earth elements. The Terani Formation samples of the REE pattern, elemental ratio, discriminate function diagram, various bivariate, and ternary plots indicate the contribution of sediments from felsic and intermediate source rocks.

The comparison of REE patterns and Eu anomalies to the source rocks from the adjacent areas reveals that the Terani clastic rocks received detritus from the Dharwar Craton. We therefore conclude that the REE patterns and Eu anomalies are well-preserved in the Terani clastic rocks and are highly reliable indicators of source rocks. The geochemical composition of Terani clastic rocks reveals a passive margin setting, which is consistent with the general geology of the Cauvery Basin.

**Acknowledgements:** This research was supported by the DST–INSPIRE Fellowship awarded to Subin Prakash (IF 140295), Ref No. DST/INSPIRE Fellowship/2014. The authors would like to thank the technicians at the Petrography and X-Ray fluorescence laboratories at the National Centre for Earth Science Studies – Trivandrum, Kerala and also to the Council of Scientific and Industrial Research (CSIR), National Geophysical Research Institute (NGRI), Hyderabad, India for geochemical analysis by High resolution inductively-coupled mass Spectrometer (HR–ICP–MS). The authors are thankful to the Head of the Department of Geology of the University of Madras for providing the necessary facilities during the course of this study.

## References

Al-Jaberi M.H. & Al-Jafar M.Kh. 2020: Elements distribution for the upper sandstone member of the Zubair Formation in Zubair oil Field, Southern Iraq. *Iraqi Geological Journal* 53 (1E), 55–74.

Alexandrowicz W.P. 2019: Malacological evidence of the natural and anthropogenic changes of the environment in the eastern part of the Carpathian foreland: The studies in the Glinne stream valley

near Rzeszów (Southern Poland). Carpathian *Journal of Earth and Environmental Sciences* 14, 367–384. https://doi.org/10.26471/cjees/2019/014/087

Allen P., Condie K.C. & Narayana B.L. 1985: Geochemistry of prograde and retrograde charnockite-gneiss reactions in southern India. *Geochimica et Cosmochimica Acta* 49, 323–336. https://doi.org/10.1016/0016-7037(85)90026-2

Anaya-Gregorio A., Armstrong-Altrin J.S., Machain-Castillo M.L., Montiel-García P.C. & Ramos-Vázquez M.A. 2018: Textural and geochemical characteristics of late Pleistocene to Holocene fine-grained deep-sea sediment cores (GM6 and GM7), recovered from southwestern Gulf of Mexico. *Journal of Palaeogeography* 7, 253–271. https://doi.org/10.1186/s42501-018-0005-3

Armstrong-Altrin J.S. 2009: Provenance of sands from Cazones, Acapulco, and Bahía Kino beaches, Mexico. *Revista Mexicana de Ciencias Geológicas* 26, 764–782.

Armstrong-Altrin J.S. 2015: Evaluation of two multi-dimensional discrimination diagrams from beach and deep sea sediments from the Gulf of Mexico and their application to Precambrian clastic sedimentary rocks. *International Geology Review* 57, 1446–1461. https://doi.org/10.1080/00206814.2014.936055

Armstrong-Altrin J.S. 2020: Detrital zircon U–Pb geochronology and geochemistry of the Riachuelos and Palma Sola beach sediments, Veracruz State, Gulf of Mexico: a new insight on palaeoenvironment. *Journal of Palaeogeography* 9. https://doi.org/10.1186/s42501-020-00075-9

Armstrong-Altrin J.S. & Machain-Castillo M.L. 2016: Mineralogy, geochemistry, and radiocarbon ages of deep sea sediments from the Gulf of Mexico, Mexico. *Journal of South American Earth Sciences* 71, 182–200. https://doi.org/10.1016/j.jsames.2016.07.010

Armstrong-Altrin J.S., Lee Y.I., Verma S.P. & Ramasamy S. 2004: Geochemistry of sandstones from the Upper Miocene Kudankulam Formation, southern India: implications for provenance, weathering, and tectonic setting. *Journal of Sedimentary Research* 74, 285–297. https://doi.org/10.1306/082803740285

Armstrong-Altrin J.S., Lee Y.I., Kasper-Zubillaga J.J., Carranza-Edwards A., Garcia D., Eby N., Balaram V. & Cruz-Ortiz N.L. 2012: Geochemistry of beach sands along the Western Gulf of Mexico, Mexico: implication for provenance. *Chemie Der Erde Geochemistry* 72, 345–362. https://doi.org/10.1016/j.chemer.2012.07.003

Armstrong-Altrin J.S., Machain-Castillo M.L., Rosales-Hoz L., Carranza-Edwards A., Sanchez-Cabeza J.A. & Ruíz-Fernández A.C. 2015: Provenance and depositional history of continental slope sediments in the Southwestern Gulf of Mexico unraveled by geochemical analysis. *Continental Shelf Research* 95, 15–26. https://doi.org/10.1016/j.csr.2015.01.003

Armstrong-Altrin J.S., Lee Y.I., Kasper-Zubillaga J.J. & Trejo-Ramírez E. 2017: Mineralogy and geochemistry of sands along the Manzanillo and El Carrizal beach areas, southern Mexico: implications for palaeoweathering, provenance and tectonic setting. *Geological Journal* 52, 559–582. https://doi.org/10.1002/gj.2792

Armstrong-Altrin J.S., Ramos-Vázquez M.A., Zavala-León A.C. & Montiel-García P.C. 2018: Provenance discrimination between Atasta and Alvarado beach sands, western Gulf of Mexico, Mexico: Constraints from detrital zircon chemistry and U–Pb geochronology. *Geological Journal* 53, 2824–2848.

Armstrong-Altrin J.S., Botello A.V., Villanueva S.F., & Soto L.A. 2019: Geochemistry of surface sediments from the northwestern Gulf of Mexico: implications for provenance and heavy metal contamination. *Geological Quarterly* 63, 522–538.

Armstrong-Altrin J.S., Ramos-Vázquez M.A., Hermenegildo-Ruiz N.Y. & Madhavaraju J. 2020: Microtexture and U–Pb geochronology of detrital zircon grains in the Chachalacas beach, Veracruz State, Gulf of Mexico. *Geological Journal*. https://onlinelibrary.wiley.com/doi/abs/10.1002/gj.3984

Asiedu D.K., Suzuki S., Nogami K. & Shibata T. 2000: Geochemistry of Lower Cretaceous sediments, inner zone of southwest Japan: constraints on provenance and tectonic environment. *Geochemical Journal* 34, 155–173.

Ayala-Pérez M.P, Armstrong-Altrin J.S. & Machain-Castillo M.L. 2021: Heavy metal contamination and provenance of sediments recovered at the Grijalva River delta, southern Gulf of Mexico. *Journal of Earth System Science*. https://doi.org/10.1007/s12040-021-01570-w.

Balaram V. 2020: Current and emerging analytical techniques for geochemical and geochronological studies. *Geological Journal*. https://doi.org/10.1002/gj.4005

Bandopadhyay P.C. & Ghosh B. 2015: Provenance analysis of the Oligocene turbidites (Andaman Flysch), South Andaman Island: a geochemical approach. *Journal of Earth System Science* 124, 1019–1037. https://doi.org/10.1007/s12040-015-0586-5

Banerji R.K. 1972: Stratigraphy and micropalaeontology of the Cauvery Basin, Part I, Exposed area. *Journal of the Palaeontological Society of India* 17, 1–24.

Basu A. 1976: Petrology of Holocene fluvial sand derived from plutonic source rocks: implications to paleoclimatic interpretation. *Journal of Sedimentary Petrology* 46, 694–709. https://doi.org/10.1306/212F7031-2B24-11D7-8648000102C1865D

Basu A. 2020: Chemical weathering, first cycle quartz sand, and its bearing on quartz arenite. *Journal Indian Association of Sedimentologists* 37, 3–14. https://doi.org/10.51710/jias.v37i2.161

Bessa A.Z.E., Nguetchoua G., Janpou A.K., El-Amier Y.A., Nguetnga O.N.N.M., Kayou U.R., Bisse S.B., Mapuna E.C.N. & Armstrong-Altrin J.S. 2020: Heavy metal contamination and its ecological risks in the beach sediments along the Atlantic Ocean (Limbe coastal fringes, Cameron). *Earth Systems and Environment.* https://doi.org/10.1007/s41748-020-00167-5

Bessa A.Z.E., Paul-Désiré N., Fuh G.C., Armstrong-Altrin J.S. & Betsi T.B. 2021: Mineralogy and geochemistry of the Ossa lake Complex sediments, Southern Cameroon: Implications for paleoweathering and provenance. *Arabian Journal of Geosciences.* https://doi.org/10.1007/s12517.021-06591-9

Bhatia M.R. 1983: Plate tectonics and geochemical composition of sandstones. *Journal of Geology* 91, 611–627. https://www.jstor.org/stable/30075206

Biswas S.K. 1993: Geology of Kutch – A compilation of Field Reports (1957–1972). *KDM Institute of Petroleum Exploration*, Dehradun, 1–450. https://doi.org/10.1007/s12594-018-1036-1

Blanford H.F. 1862: On the Cretaceous and other rocks of the South Arcot and Trichinopoly districts. *Memoir Geological Society of India*, 1–217.

Carver R.E. 1971: Procedures in Sedimentary Petrology. Wiley Interscience, New York, 1–653.

Chacko T., Ravindra Kumar G.R., Meen J.K. & Rogers J.W. 1992: Geochemistry of high-grade supracrustal rocks from the Kerala Khondalite Belt and adjacent massif charnockites, South India. *Precambrian Research* 55, 469–489. https://doi.org/10.1016/0301-9268(92)90040-U

Condie K.C. 1993: Chemical composition and evolution of the upper continental crust: contrasting results from surface samples and shales. *Chemical Geology* 104, 1–37. https://doi.org/10.1016/0009-2541(93)90140-E

Cox R., Lowe D.R. & Cullers R.L. 1995: The influence of sediment recycling and basement composition on evolution of mudrock chemistry in the southwestern United States. *Geochimica et Cosmochimica Acta* 59, 2919–2940. https://doi.org/10.1016/0016-7037(95)00185-9

Cullers R.L. 1994: The chemical signature of source rocks in size fractions of Holocene stream sediment derived from metamorphic rocks in the wet mountains region, Colorado, USA.

*Chemical Geology* 113, 327–343. https://doi.org/10.1016/0009-2541(94)90074-4

Cullers R.L. 2000: The geochemistry of shales, siltstones and sandstones of Pennsylvanian–Permian age, Colorado, USA: implications for provenance and metamorphic studies. *Lithos* 51, 181–203. https://doi.org/10.1016/S0024-4937(99)00063-8

Cullers R.L. 2002: Implications of elemental concentrations for provenance, redox conditions, and metamorphic studies of shales and limestones near Pueblo, CO, USA. *Chemical Geology* 191, 305–327. https://doi.org/10.1016/S0009-2541(02)00133-X

Cullers R.L. & Podkovyrov V.N. 2000: Geochemistry of the Mesoproterosoic Lakhanda shales in southern Yakutia, Russia: implications for mineralogical and provenance control, and recycling. *Precambrian Research* 104, 77–93.

Cullers R.L., Basu A. & Suttner L. 1988: Geochemical signature of provenance in sand-size material in soils and stream sediments near the Tobacco Root batholith, Montana, USA. *Chemical Geology* 70, 335–348.

Cusack M., Arrieta J.M. & Duarte C.M. 2020: Source apportionment and elemental composition of atmospheric total suspended particulates (TSP) over the Red Sea coast of Saudi Arabia. *Earth Systems and Environment* 4, 777–788. https://doi.org/10.1007/s41748-020-00189-z

Damian G., Iepure Z.S.G. & Damian F. 2019: Distribution of heavy metals in granulometric fractions and on soil profiles. *Carpathian Journal of Earth and Environmental Sciences* 14, 343–351. https://doi.org/10.26471/cjees/2019/014/085

Dey S., Rai A.K. & Chaki A. 2009: Palaeoweathering, composition and tectonics of provenance of the Proterozoic intracratonic Kaladgi–Badami basin, Karnataka, southern India: Evidence from sandstone petrography and geochemistry. *Journal of Asian Earth Sciences* 34, 703–715. https://doi.org/10.1016/j.jseaes.2008.10.003

Dickinson W.R. 1985: Interpreting provenance relations from detrital modes of sandstones. In: Zuffa, G.G. (Eds.), Provenance of Arenites. Springer, Dordrecht. 333–361. https://doi.org/10.1007/978-94-017-2809-6_15

Etemad-Saeed N., Hosseini-Barzi M., Adabi M.H., Sadeghi A. & Houshm Zadeh A. 2015: Provenance of Neoproterozoic sedimentary basement of northern Iran, Kahar Formation. *Journal of African Earth Science* 111, 54–75. https://doi.org/10.1016/j.jafrearsci.2015.07.003

Fedo C.M., Nesbitt H.W. & Young G.M. 1995: Unraveling the effect of potassium metasomatism in sedimentary rocks and paleosols, with implications for paleoweathering conditions and provenance. *Geology* 23, 921–924. https://doi.org/10.1130/0091-7613(1995)023%3C0921:UTEOPM%3E2.3.CO;2

Feng R. & Kerrich R. 1990: Geochemistry of fine-grained clastic sediments in the Archean Abitibi greenstones belt, Canada: implications for provenance and tectonic setting. *Geochimica et Cosmochimica Acta* 54, 1061–1081. https://doi.org/10.1016/0016-7037(90)90439-R

Folk R.L. 1980: Petrology of Sedimentary Rocks. *Hemphill*, Austin, Texas, 1–159.

Garver J.I., Royce, P.R. & Smick T.A. 1996: Chromium and nickel in shale of the Taconic foreland: a case study for the provenance of fine-grained sediments with an ultramafic source. *Journal of Sedimentary Research* 66, 100–106. https://doi.org/10.1306/D42682C5-2B26-11D7-8648000102C1865D

George-Marian I., Roba C., Bălc R. & Maria Gligor D. 2020: The content of nutrients and contaminants in soil and vegetables cultivated in several greenhouses from Botoșani county and their impact on human health. *Carpathian Journal of Earth and Environmental Sciences.* 15, 415–428. https://doi.org/10.26471/cjees/2020/015/141

Govindan A., Ravindran C.N. & Rangaraju M.K. 1996: Cretaceous stratigraphy and planktonic foraminiferal zonation of Cauvery Basin, South India. In: A. Sahni (Ed.): Cretaceous Stratigraphy and Palaeoenvironments. *Memoir of Geological Society of India,* 1–32.

Harnois L. 1988: The CIW index: a new chemical index of weathering. *Sedimentary Geology* 55, 319–322. https://doi.org/10.1016/0037-0738(88)90137-6

Hayashi K.I., Fujisawa H., Holland H.D. & Ohmoto H. 1997: Geochemistry of ~1.9 Ga sedimentary rocks from northeastern Labrador, Canada. *Geochimica et Cosmochimica Acta* 16, 4115–4137. https://doi.org/10.1016/s0016-7037(97)00214-7

Hernández-Hinojosa V., Montiel-García P.C., Armstrong-Altrin J.S., Nagarajan N. & Kasper-Zubillaga J.J. 2018: Textural and geochemical characteristics of beach sands along the western Gulf of Mexico, Mexico. *Carpathian Journal of Earth and Environmental Sciences.* 13, 161–174. http://hdl.handle.net/20.500.11937/55468

Hossain H.M.Z., Armstrong-Altrin J.S., Jamil A.H.M.N., Rahman M.M., Hernández-Coronado, C.J. & Ramos-Vázquez M.A. 2020: Microtextures on quartz grains in the Kuakata beach, Bangladesh: implications for provenance and depositional environment. *Arabian Journal of Geosciences* 13, 291. https://doi.org/10.1007/s12517-020-5265-4

Hu G., Hu W.X., Cao J., Yang R.F., Chen H.Y., Zhao D.F., Pang Q., Wang H.Y. & Tan X.C. 2017: The distribution, hydrocarbon potential, and development of the Lower Cretaceous black shales in coastal southeastern China. *Journal of Palaeogeography* 6, 333–351. https://doi.org/10.1016/j.jop.2017.08.002

Imchen W., Glenn Thong T. & Temjenrenla P. 2014: Provenance, tectonic setting and age of the sediments of the upper Disang formation in the Phek District, Nagaland. *Journal of Asian Earth Sciences* 88, 11–27.

Ingersoll R.V., Bullard T.F., Ford R.L., Grimm J.P., Pickle J.D. & Sares S.W. 1984: The effect of grain size on detrital modes: a test of the Gazzi–Dickinson point counting method. *Journal of Sedimentary Petrology* 54, 0103–0116. https://doi.org/10.1306/212F83B9-2B24-11D7-8648000102C1865D

Jamwal M., Pandita S.K., Sharma M. & Bhat G.M. 2020: Petrography, provenance and diagenesis of Murree Group of rocks exposed along Basohli – Bani road, Kathua, Jammu. *Journal Indian Association of Sedimentologists* 37, 15–26. https://doi.org/10.51710/jias.v37i2.79

Jayananda M., Martin H., Peucat J.J. & Mahabaleswar B. 1995: Late Archaean crust-mantle interactions: geochemistry of LREE-enriched mantle derived magmas. Example of the Clospet batholith, southern India. *Contribution to Mineralogy and Petrology* 119, 314–329. https://doi.org/10.1007/BF00307290

Karlik M., Gyollai I., Vancsik A., Fintor K., Szalai Z., Mîndrescu M., Grădinaru I., Vágási S., Bozsó G., Polgári M. & Pál-Molnár E. 2021: High resolution mineralogical characterization of sediments – lake Bolătău-Feredeu (Romania). *Carpathian Journal of Earth and Environmental Sciences* 16, 199–210. https://doi.org/10.26471/cjees/2021/016/167

Kasanzu C., Maboko M.A.H. & Manya S. 2008: Geochemistry of fine grained clastic sedimentary rocks of the Neoproterozoic Ikorongo Group, NE Tanzania: Implications for provenance and source rock weathering. *Precambrian Research* 201–213. https://doi.org/10.1016/j.precamres.2008.04.007

Kettanah Y.A., Armstrong-Altrin J.S., Mohammad F.A. 2020: Petrography and geochemistry of siliciclastic rocks of the Middle Eocene Gercus Formation, northern Iraq: Implications for provenance and tectonic setting. *Geological Journal.* https://doi.org/10.1002/gj.3880

Krishnan G., Nagendra R., Elango L., Narasimha K.N.P., Vybhav K. & Mujumdar M. 2020: Spatial and Temporal Variations in Geo-

chemistry of Cauvery River Sediments (Tamilnadu, India): Indicators of Provenance and Weathering. *Journal Indian Association of Sedimentologists* 37, 49–60. https://doi.org/10.51710/jias.v37i2.107

Li F., Ma W., Meng F. & Diao H. 2020: Geochemical characteristics and geological significance of Daohugou Formation at Ningcheng County of Inner Mongolia, eastern China. *Geological Journal*. https://doi.org/10.1002/gj.4050

Ma A., Hu X., Kapp P.A., Han Z., Lai W. & BouGagher-Fadel M. 2018: The disappearance of a Late Jurassic remnant sea in the southern Qiangtang Block (Najiangco area): Implications for the tectonic uplift of central Tibet. *Palaeogeography, Palaeoclimatology, Palaeoecology* 506, 30–47. https://doi.org/10.1016/j.palaeo.2018.06.005

Mack G.H. & Suttner L.J. 1977: Paleoclimate interpretation from a petrographic comparison of Holocene sands and the Fountain Formation (Pennsylvanian) in the Colorado Front Range. *Journal of Sedimentary Petrology* 47, 89–100. https://doi.org/10.1306/212F70FE-2B24-11D7-8648000102C1865D

Madhavaraju J. 2015: Geochemistry of late Cretaceous sedimentary rocks of the Cauvery Basin, south India: constraints on paleoweathering, provenance, and end Cretaceous environments. *Chemostratigraphy* 185–214. https://doi.org/10.1016/B978-0-12-419968-2.00008-X

Madhavaraju J. & Lee Y.I. 2010: Influence of Deccan volcanism in the sedimentary rocks of Late Maastrichtian–Danian age of Cauvery basin Southeastern India: constraints from geochemistry. *Current Science* 98, 528–537. https://www.jstor.org/stable/24111704

Madhavaraju J., Armstrong-Altrin J.S., Pillai R.B. & Pi-Puig T. 2020: Geochemistry of sands from the Huatabampo and Altata beaches. Gulf of California, Mexico. *Geological Journal*. https://doi.org/10.1002/gj.3864

Maftei A-E., Buzgar N., Buzat A. & Apopei A-I. 2019: Distribution and minor elements contamination in urban and Peri-Uban soils area of Slănic Moldova, Romania. *Carpathian Journal of Earth and Environmental Sciences* 14, 335–342. https://doi.org/10.26471/cjees/2019/014/084

McLennan S.M. 2001: Relationships between the trace element composition of sedimentary rocks and upper continental crust. *Geochemistry Geophysics Geosystems* 2, 2000GC000109. https://doi.org/10.1029/2000GC000109

McLennan S.M & Taylor S.R. 1991: Sedimentary-Rocks and Crustal Evolution: Tectonic Setting and Secular Trends. *Journal of Geology* 99, 1–21. https://doi.org/10.1086/629470

McLennan S.M., Nance W.B. & Taylor S.R. 1980: Rare earth element–Thorium correlation in sedimentary rocks, and the composition of the continental crust. *Geochimica et Cosmochimica Acta* 44, 1833–1839. https://doi.org/10.1016/0016-7037(80)90232-X

McLennan S.M., Hemming S., McDaniel D.K. & Hanson G.N. 1993: Geochemical approaches to sedimentation, provenance and tectonics. In: Johnsson M.J. & Basu A. (Eds.): Processes Controlling the Composition of Clastic Sediments. *Geological Society of America* 21–40 (Special Paper 284). https://doi.org/10.1130/SPE284-p21

Middleton G.V. 1972: Albite of secondary origin in Charny sandstones, Quebec. *Journal of Sedimentary Petrology* 42, 341–349. https://doi.org/10.1306/212F7CE8-2B24-11D7-8648000102C1865D

Mongelli G., Critelli S., Perri F., Sonnino M. & Perrone V. 2006: Sedimentary recycling, provenance and paleoweathering from chemistry and mineralogy of Mesozoic continental redbed mudrocks, Peloritani mountains, southern Italy. *Journal of Geochemistry* 40, 197–209. https://doi.org/10.2343/geochemj.40.197

Morton A.C., Whitham A.G. & Fanning C.M. 2005: Provenance of Late Cretaceous to Paleocene submarine fan sandstones in the Norwegian Sea: integration of heavy mineral, mineral chemical and zircon age data. *Sedimentary Geology* 182, 3–28.

Mude S.N., Yawale S. & Choudhari V. 2020: Sedimentological and geochemical charecterization of Manaveli and Cuddalore Formations, Puducherry Basin, India. *Journal Indian Association of Sedimentologists* 37, 115–130. https://doi.org/10.51710/jias.v37i2.112

Mustafa R.K. & Tobia F.H. 2020: Geochemical application in unraveling paleoweathering, provenance and environmental setting of the shale from Chia Gara Formation, Kurdistan Region, Iraq. *Iraqi Geological Journal* 53 (1A), 90–116.

Nagarajan R., Armstrong-Altrin J.S., Kessler F.L., Hidalgo-Moral E.L., Dodge–Wan D. & Taib N.I. 2015: Provenance and tectonic setting of Miocene siliciclastic sediments, Sibuti Formation, northwestern Borneo. *Arabian Journal of Geosciences* 8, 8549–8565. https://doi.org/10.1007/s12517-015-1833-4

Nagendra R., Kamalak Kannan B.V., Sen G., Gilbert H., Bakkiaraj D., Nallapa Reddy A. & Jaiprakash B.C. 2011: Sequence surfaces and paleobathymetric trends in Albian to Maastrichtian sediments of Ariyalur area, Cauvery Basin, India. *Marine and Petroleum Geology* 28, 895–905. https://doi.org/10.1016/j.marpetgeo.2010.04.002

Nesbitt H.W. & Young G.M. 1982: Early Proterozoic climates and plate motions inferred from major element chemistry of lutites. *Nature* 299, 715–717. https://doi.org/10.1038/299715a0

Paikaray S., Banerjee S. & Mukherjee S. 2008: Geochemistry of shales from the Paleoproterozoic to Neoproterozoic Vindhyan Supergroup: implications on provenance, tectonics and paleoweathering. *Journal of Asian Earth Sciences* 32, 34–48. https://doi.org/10.1016/j.jseaes.2007.10.002

Prabhakar K.N. & Zutchi P.L. 1993: Evolution of southern part of Indian East Coast basins. *Journal of Geological Society of India* 41, 215–230.

Rahman M.J.J., Sayem A.S.M. & McCann T. 2014: Geochemistry and provenance of the Miocene sandstones of the Surma Group from the Sitapahar anticline, Southeastern Bengal Basin, Bangladesh. *Journal of Geological Society of India* 83, 447–456. https://doi.org/10.1007/s12594-014-0061-y

Ramasamy S. & Banerji R.K. 1991: Geology, petrography and stratigraphy of pre–Ariyalur sequence in Tiruchirapalli District, Tamil Nadu. *Journal of Geological Society of India* 37, 577–594.

Ramos-Vázquez M.A., Armstrong-Altrin J.S., Machain-Castillo M.L. & Gío-Argáez F.R. 2018: Foraminiferal assemblages, $^{14}C$ ages, and compositional variations in two sediment cores in the western Gulf of Mexico. *Journal of South American Earth Sciences* 88, 480–496. https://doi.org/10.1016/j.jsames.2018.08.025

Ramos-Vázquez M.A. & Armstrong-Altrin J.S. 2019: Sediment chemistry and detrital zircon record in the Bosque and Paseo del Mar coastal areas from the southwestern Gulf of Mexico. *Marine and Petroleum Geology* 110, 650–675.

Ramos-Vázquez M.A. & Armstrong-Altrin J.S. 2020: Provenance and palaeoenvironmental significance of microtextures in quartz and zircon grains from the Paseo del Mar and Bosque beaches, Gulf of Mexico. *Journal of Earth System Science* 129, 225 https://doi.org/10.1007/s12040-020-01491-0

Ramos-Vázquez M.A., Armstrong-Altrin J.S., Rosales-Hoz L., Machain-Castillo M.L. & Carranza-Edwards A. 2017: Geochemistry of deep-sea sediments in two cores retrieved at the mouth of the Coatzacoalcos river delta, Western Gulf of Mexico, Mexico. *Arabian Journal of Geosciences* 10, 148. https://doi.org/10.1007/s12517-017-2934-z

Rivera-Gómez M.A., Armstrong-Altrin J.S., Verma S.P. & Díaz-González L. 2020: APMDisc: An online computer program for the geochemical discrimination of siliciclastic sediments from

active and passive margins. *Turkish Journal of Earth Sciences* 29, 550–578. https://doi.org/10.3906/yer-1908-15

Roddaz M., Viers J., Brusset S., Baby P., Boucayrand C. & Hérail G. 2006: Controls on weathering and provenance in the Amazonian foreland basin: Insights from major and trace element geochemistry of Neogene Amazonian sediments. *Chemical Geology* 226, 31–65. https://doi.org/10.1016/j.chemgeo.2005.08.010

Roser B.P. & Korsch R.J. 1986: Determination of tectonic setting of sandstone mudstone suites using $SiO_2$ content and $K_2O/Na_2O$ ratio. *Journal of Geology* 94, 635–650. https://doi.org/10.1086/629071

Rudnick R. & Gao S. 2003: Composition of the continental crust. *Treatise on Geochemistry* 3, 1–64. https://doi.org/10.1016/B0-08-043751-6/03016-4

Sastry M.V.A., Mamgain V.D. & Rao B.R. 1972: Ostracod fauna of the Ariyalur Group (Upper Cretaceous) Tiruchirapalli District, Tamil Nadu. Part I. Lithostratigraphy of the Ariyalur Group. Memoir *Geological Survey of India, Palaeontological Indica, New Series*, 1–48.

Satyanarayanan M., Balaram V., Sawant S.S., Subramanyam K.S.V. & Vamsi Krishna G. 2014: High precision multi element analysis on geological samples by HR–ICP–MS, 28th ISMAS-WS: 28th ISMAS Symposium Cum Workshop on Mass Spectrometry, Timber Trail Height, Parwanoo, Himachal Pradesh, India, March 9–13, 181–184.

Scarciglia F., Critelli S., Borrelli L., Coniglio S., Muto F. & Perri F. 2016: Weathering profiles in granitoid rocks of the Sila Massif uplands, Calabria, southern Italy: New insights into their formation processes and rates. *Sedimentary Geology* 336, 46–67. https://doi.org/10.1016/j.sedgeo.2016.01.015

Srivastava R.P. & Tewari B.S. 1967: Biostratigraphy of the Ariyalur Stage, Cretaceous of Trichinopoly. *Journal of Paleontological Society of India* 12, 48–54.

Stähle H.J., Raith M., Hoernes S. & Delfs A. 1987: Element mobility during incipient granulite formation at Kabbaldurga, southern India. *Journal of Petrology* 28, 803–834. https://doi.org/10.1093/petrology/28.5.803

Subin Prakash R., Ramasamy S. & Namitha Mary Varghese. 2018: Provenance of the Gondwana sediments, Palar Basin, Southern India. *Arabian Journal of Geosciences* 11, 163. https://doi.org/10.1007/s12517-018-3494-6

Sundaram R. & Rao P.S. 1986: Lithostratigraphy of the Upper Cretaceous rocks in the Vridhachalam area, south Arcot district, Tamil Nadu, South India. *Geological Survey of India, Special Publication* 11, 515–522.

Sundaram R., Henderson R.A., Ayyasami K. & Stilwell J.D. 2001: A lithostratigraphic revision and palaeo-environmental assessment of the Cretaceous system exposed in the onshore Cauvery Basin, southern India. *Cretaceous Research* 22, 743–762. https://doi.org/10.1006/cres.2001.0287

Suttner L.J. 1974: Sedimentary petrographic provinces: An evaluation. *SEPM Special Publication* 21, 75–84. https://doi.org/10.2110/pec.74.21.0136

Suttner L.J., Basu A. & Mack G.H. 1981: Climate and the origin of quartz arenite. *Journal of Sedimentary Petrology* 51, 1235–1246. https://doi.org/10.1306/212F7E73-2B24-11D7-8648000102C1865D

Tanner L.H. & Lucas S.G. 2017: Paleosols of the upper Paleozoic Sangre de Cristo Formation, north-central New Mexico: Record of early Permian palaeoclimate in tropical Pangaea. *Journal of Palaeogeography* 6, 144–161. https://doi.org/10.1016/j.jop.2017.02.001

Tapia-Fernandez H.J., Armstrong-Altrin J.S. & Selvaraj K. 2017: Geochemistry and U-Pb geochronology of detrital zircons in the Brujas beach sands, Campeche, Southwestern Gulf of Mexico, Mexico. *Journal of South American Earth Sciences* 76, 346–361. https://doi.org/10.1016/j.jsames.2017.04.003

Taylor S.R. & McLennan S.M. 1985: The Continental Crust: Its Composition and Evolution. *Blackwell Scientific Publications*, London, 1–312.

Tewari A., Hart M.B. & Watkinson M.P. 1996: A revised lithostratigraphic classification of the Cretaceous rocks of the Trichinopoly district, Cauvery Basin, Southeast India. In: Pandey J., Azmi R.J., Bhandari A. & Dave A. (Eds.): Contributions to the XV Indian Colloquium on Micropalaeontology and Stratigraphy, 789–800.

Tijani M.N., Nton M.E. & Kitagawa R. 2010: Textural and geochemical characteristics of the Ajali Sandstone. Anabra Basin, SE Nigeria: Implication for its provenance. *Comptes Rendus Geoscience* 342, 136–150. https://doi.org/10.1016/j.crte.2009.09.009

Tobia F.H. & Aswad K.J. 2015: Petrography and geochemistry of Jurassic sandstones, Western Desert, Iraq: implications on provenance and tectonic setting. *Arabian Journal of Geosciences* 8, 2771–2784. https://doi.org/10.1007/s12517-014-1392-0

Veena M.P., Achyuthan H., Eastoe C. & Farooqui A. 2014: A multiproxy reconstruction of monsoon variability in the late Holocene, South India. *Quaternary International* 325, 63–73. https://doi.org/10.1016/j.quaint.2013.10.026

Verlekar P. & Kotha M. 2020: Provenance, tectonics and palaeoenvironment of Mesoproterozoic Saundatti Quartzite Member of Kaladgi Basin, India: a petrographic view. *Journal Indian Association of Sedimentologists* 37, 91–102.

Verma S.P. & Armstrong-Altrin J.S. 2013: New multi-dimensional diagrams for tectonic discrimination of siliciclastic sediments and their application to Precambrian basins. *Chemical Geology* 355, 117–133. https://doi.org/10.1016/j.chemgeo.2013.07.014

Verma S.P. & Armstrong-Altrin J.S. 2016: Geochemical discrimination of siliciclastic sediments from active and passive margin settings. *Sedimentary Geology* 332, 1–12. https://doi.org/10.1016/j.sedgeo.2015.11.011

Yang J.H. & Du Y.S. 2017: Weathering geochemistry and palaeoclimate implication of the Early Permian mudstones from eastern Henan Province, North China. *Journal of Palaeogeography* 6, 370–380. https://doi.org/10.1016/j.jop.2017.08.003

Zaid S.M., EL-Badry O.A., Akarish A.M. & Mohamed M.A. 2018: Provenance, weathering, and paleoenvironment of the Upper Cretaceous Duwi black shales, Aswan Governorate, Egypt. *Arabian Journal of Geosciences* 11, 147. https://doi.org/10.1007/s12517-018-3500-z

Zeng S., Wang J., Fu X., Chen W., Song C., Feng X. & Wang D. 2020: Geochemistry and detrital zircon geochronology of the Jurassic clastic rocks of the northern Qiangtang Basin, northern Tibet: Implication for palaeoenvironment, provenance, and tectonic setting. *Geological Journal.* https://doi.org/10.1002/gj.4074

Zhang Y. & Gao X. 2015: Rare earth elements in surface sediments of a marine coast under heavy anthropogenic influence: the Bohai Bay, China. *Estuary Coastal Shelf Science* 164, 86–93. https://doi.org/10.1016/j.ecss.2015.07.017

Zhou L., Friis H. & Poulsen M.L.K. 2015: Geochemical evaluation of the Late Paleocene and Early Eocene shales in Siri Canyon, Danish–Norwegian Basin. *Marine and Petroleum Geology* 61, 111–122. https://doi.org/10.1016/j.marpetgeo.2014.12.014

Znad R.Kh., Al-Khatony S.E. & Al-Sumaidaie M.A.H. 2020: Effect of tectonic setting on distribution of pelagic sediment unit (Shiranish Formation) in Zagros Foreland Basin, Iraqi Segment. *Iraqi Geological Journal* 53 (2A), 105–119.